HYDRODYNAMICS AND MOMENTUM DISTRIBUTION OF PRODUCED HADRONS IN HIGH ENERGY HEAVY-ION COLLISIONS

A Thesis Submitted
in Partial Fulfilment of the Requirements
for the Degree of

MASTER OF SCIENCE

by

EVAN JOHN PHILIP

to the

School of Physical Sciences

National Institute of Science Education and Research

Bhubaneswar

Date

DECLARATION

I hereby declare that I am the sole author of this thesis in partial fulfilment of the requirements for a postgraduate degree from National Institute of Science Education and Research (NISER). I authorize NISER to lend this thesis to other institutions or individuals for the purpose of scholarly research.

Signature of the Student
Date:

The thesis work reported in the thesis entitled *Understanding the Momentum Distribution of Produced Hadrons in High Energy Collisions : Random Walk Model versus Blast Wave Model* was carried out under my supervision, in the School of Physical Sciences at NISER, Bhubaneswar, India.

Signature of the thesis supervisor
School:
Date:

ACKNOWLEDGEMENTS

I consider it an honour to have had the opportunity to be supervised by Prof. Bedangadas Mohanty. His support, in spite of his hectic schedule, was always unstinted, be it in project related matters or in times of personal crisis. There were countless occasions on which he clarified my doubts over phone or over Skype during late hours. His association with me has not only been that of a supervisor but also that of an indispensable mentor. He led by example. Without him, I would not have been where I am today.

ABSTRACT

The transverse momentum distribution of hadrons produced in heavy ion collisions over a wide range of centre-of-mass energy (9 GeV to 2760 GeV) has been compared to the *random walk model*, which is based on the assumption that a nucleus-nucleus (A-A) collision is the superposition of isotropically decaying thermal sources at a given freeze out temperature. The freeze out temperature in A-A collisions is fixed from the inverse slope of the transverse momentum spectra of hadrons in nucleon-nucleon (p-p) collision. Successive collisions, like in case of nucleon-nucleus (p-A) collision, leads to gain in transverse momentum, as the nucleons are assumed to propagate in the nucleus following a random walk pattern. The average transverse rapidity shift per collision is determined from the p-A collision data. Using this information, we obtain a parameter free result for the transverse momentum distribution of produced hadrons in A-A collision.

It is observed that the random walk model is able to explain the transverse momentum spectra of produced particles, especially the lighter pions, at lower energies. However, it fails to explain the transverse momentum distribution of hadrons at higher energies. This indicates the presence of additional physical effects, like a collective phenomena, which cannot be accounted for by the initial state collision broadening of transverse momentum of produced hadrons, which is the basis of random walk model. In support of this later phenomena we, present a model inspired by hydrodynamic modelling of A-A collisions. This model, called *blast wave model*, satisfactorily explains the transverse momentum distribution of produced hadrons in A-A collisions across all the beam energies studied.

The blast wave model is a phenomenological hydrodynamics-inspired model. The application of hydrodynamics to matter created in high energy heavy-ion collisions is then studied. The time in the evolution history of heavy-ion collisions where hydrodynamics is applicable is alluded to, followed by a brief discussion on relativistic formulation of hydrodynamics. Then hydrodynamics equations are set up in 1+1 dimensions and their solutions using Bjorken initial conditions is presented. An essential input to solving these calculations is the equation of state of the matter under

consideration. A discussion follows on a range of possible equations of state, starting with a simple ideal gas equation of state, proceeding to MIT Bag Model approach and QCD based calculation using lattice gauge theory. The effect of different choices of equation of state on the time evolution of the energy density of the system is presented. The derivation of the hydrodynamic equations in a more realistic 2+1 dimensions in then discussed. Solutions to these equations can provide both momentum and azimuthal angle distribution of produced hadrons in the heavy-ion collisions. Finally, the 1+1 dimensional hydrodynamic calculations are used to convert the fluid matter to particles (Cooper-Frye algorithm) and the momentum distributions of pions and protons produced in heavy-ion collisions is looked at. The slope of pion momentum distribution is seen to be larger compared to that of protons, proving that the mass dependence of the slope of transverse momentum distribution of particles produced in heavy-ion collisions is a consequence of hydrodynamics-like behaviour of the medium formed in the collisions.

Contents

1 Introduction **1**
1.1 Heavy Ion Collisions 1
1.2 Observation of Interest 3
1.3 Conventions 5

2 Random-walk model **7**
2.1 The Model 7
2.2 Analysis 10
2.3 An Alternative Including Collectivity - Blast Wave Model 12
2.4 Conclusion 15

3 Hydrodynamics in Relativistic Heavy Ion Collsion **17**
3.1 Spacetime Evolution in Heavy Ion Collisions 18
3.2 Relativistic Hydrodynamics 19

4 Hydrodynamics in 1+1 D **24**
4.1 Simplification 24
4.2 Solution using Bjorken Initial Condition 26
4.3 Results 27

5 Equations of State **29**
5.1 Ideal Gas 29
5.2 Bag Model 30
5.2.1 The QGP Phase 31
5.2.2 The Hadron Phase 34
5.2.3 Bag Pressure 37
5.2.4 Equation of State 40
5.3 Lattice QCD 41

6 Hydrodynamics in 2+1 D **43**
6.1 Entropy Current Conservation Equation 43
6.2 Temperature Equation 44
6.3 Simplification 44
6.4 Characteristic Solution 45

7 Comparison to Experimental Output **47**
7.1 BJ HYDRO 48
7.1.1 Computation of the Hadronization Hypersurface (`bj_hydro.f`) 49
7.1.2 Generation of Particle Output from the Hypersurface (`evgen.f`) 50
7.1.3 Results 50
7.2 Outlook 51

8 Conclusion **52**

References **55**

Appendix A Fits of $p - p$ collisions using random walk model **60**

Appendix B Fits of $p - A$ collisions using random walk model **70**

Appendix C Fits of $A - A$ collisions using random walk model **74**

Appendix D Fits using blast wave model **76**

Appendix E Degrees of freedom of hadrons **78**

List of Figures

1.1 Collision of Lorentz contracted heavy nucli at relativistic speed.[2] . . . 2
1.2 Transverse momentum distribution of particle yields of different particles at 2.76 TeV in PbPb collision. 3
1.3 Transverse momentum distribution of particle yields of different particles at 5.02 TeV in pPb collision. 4
1.4 Center-of-mass scattering angle.[6] 6

2.1 10
2.2 11
2.3 12
2.4 15

3.1 Diagram depicting spacetime evolution of heavy ion collision.[13] 18

4.1 Energy density as a function of time for different equations of state. . 27

5.1 Pressure and Energy density of QGP. 34
5.2 Total pressure and energy density of mesons listed in Appendix E. . . 36
5.3 Total pressure and energy density of baryons listed in Appendix E. . 37
5.4 Pressure versus temperature, with QGP pressure (Section 5.2.1) above $T_c = 175$ MeV and hadronic pressure (Section 5.2.2) below T_c. 37
5.5 c_s^2 as a function of temperature as obtained from the bag model. . . . 40
5.6 c_s^2 as a function of temperature as obtained from lattice calculations.[23] 42

7.1 Flowchart summerising BJ HYDRO. 48
7.2 Results generated by BJ HYDRO. 51

A.1 Fits for π^+ yield in $p-p$ collisions. 61
A.2 Fits for π^- yield in $p-p$ collisions. 63
A.3 Fits for K^+ yield in $p-p$ collisions. 64
A.4 Fits for K^- yield in $p-p$ collisions. 66
A.5 Fits for p yield in $p-p$ collisions. 67
A.6 Fits for $\bar{p}$ yield in $p-p$ collisions. 69

B.1 Fits for π^+ and π^- yield in $p-A$ collisions. 71
B.2 Fits for K^+ and K^- yield in $p-A$ collisions. 72
B.3 Fits for p and $\bar{p}$ yield in $p-A$ collisions. 73

C.1 Fits for π^+ and π^- yield in $A-A$ collisions. 75
C.2 Fits for p and $\bar{p}$ yield in $A-A$ collisions. 75

D.1 Fits of particle yield in $A-A$ collisions using blast wave model. . . . 77

List of Tables

1.1 Metric value of quantities in natural unit 5

7.1 Transport coefficients and their relationship with thermodynamic quantities 51

8.1 Source of collision data used in analysis 59

E.1 Degrees of Freedom of Mesons[19] 78
E.2 Degrees of Freedom of Baryons[19] 79

Chapter 1

Introduction

1.1 Heavy Ion Collisions

Elementary physics utilises collisions to probe phenomenon which occur at a very small length scales, a technique which has made immense contributions to the field starting with Rutherford's discovery of the atomic nucleus in 1911. High energy colliders were initially designed to collide the most elementary particles known of, in order to probe their substructure. However, in late seventies and early eighties, relativistic collisions of heavier nuclei was made possible. Many particle colliders like Bevatron in Berkeley were converted to accelerate ions and the energies of existing nuclear accelerators were increased to relativistic regime[1]. By mid 80s the the highest energy proton accelerators, like the Alternating Gradient Synchrotron at Brookhaven National Laboratory and the Super Proton Synchrotron at CERN also started injecting heavy ions[1]. The injection of heavy ions into the Large Hadron Collider was planned from its initial phase[1] and towards the end of 2010 the LHC conducted its first $Pb - Pb$ collision, marking the start of its heavy ion research program.

The initial collision experiment conducted by Rutherford explored the substructure of atoms and subsequent collisions, starting from the electron-on-proton collision in 1968 at the Stanford Linear Accelerator Center, shed light on the substructure of baryons. What, then, is the reason for colliding heavy ions? The broad motivation for performing heavy ion collisions is to understand matter at high densities and temperature. However, perhaps, the main attraction in high energy heavy collisions is to produce a de-confined state of quarks and gluons, similar to that which existed in the micro-second old universe, called *quark gluon plasma*.

Deep inelastic scattering had indicated the existence of a substructure for baryons in the early seventies itself[1]. The theory for their constituents, quarks and gluons, is quantum chromodynamics[1]. Quantum chromodynamics predicts that quarks and gluons cannot be observed in their free state in physical vacuum since they are confined by strong force[1]. At high enough energy densities, this strong tie may weaken and these particles may propagate longer distances[1]. This de-confined, dense state of matter is known as *quark gluon plasma* and provide a unique arena to study and test our understanding of fundamental physics. The high temperatures and densities required to obtain this condition can be achieved in the collision of a relatively large number of particles as in heavy ion collisions.

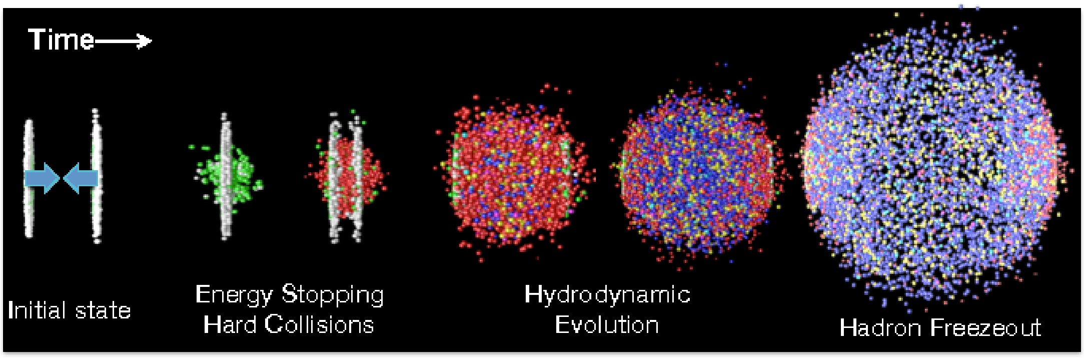

Figure 1.1: Collision of Lorentz contracted heavy nucli at relativistic speed.[2]

In heavy ion collision, nuclei up to that of lead or uranium are accelerated to relativistic speeds. The nuclei are Lorentz contracted in their direction of motion like pancakes and collide head on, as shown in Figure 1.1, forming a hot plasma, supposedly of quarks and gluons.

During the evolution of this plasma, it undergoes a range of energy densities and temperatures, and possibly different phases. Due to the thermal pressure, the plasma first undergoes an expansion and eventually becomes so dilute that it hadronizes. In the hadronic phase, it further cools down via inelastic and elastic interactions until it becomes non-interacting, a state known as *freeze-out*. We detect these hadrons. A similar, but much slower stage of evolution is thought to have existed during the evolution of the universe also.

1.2 Observation of Interest

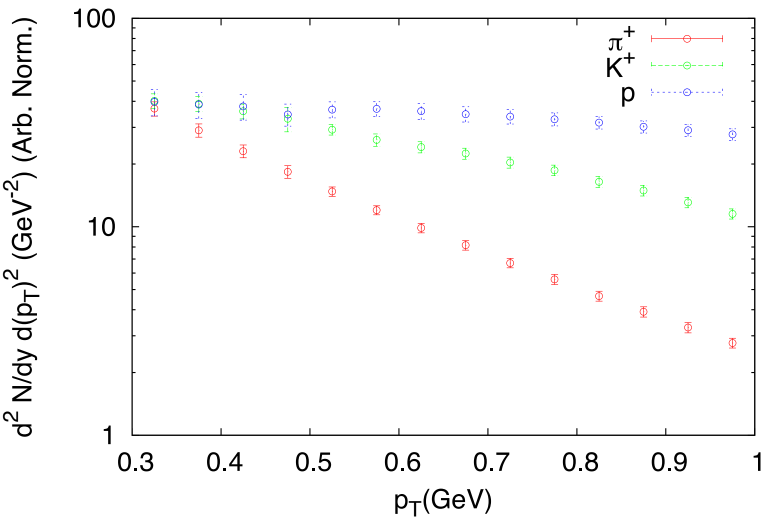

Figure 1.2: Transverse momentum distribution of particle yields of different particles at 2.76 TeV in PbPb collision.

The observation of interest in this thesis is the transverse momentum distribution of particle yields in high energy heavy ion collisions. The transverse momentum distribution of particle yields for different particle species, on a semi-log scale, shows an increasing slope with particle mass, as shown in Figure 1.2.

This feature is typical of a hydrodynamic system at thermodynamic equilibrium, and is hence an indication of a collective phenomenon. This behaviour is expected if there is formation of quark gluon plasma. However, surprisingly, the same behaviour is shown even when protons collide with nuclei, as shown in Figure 1.3, where quark-

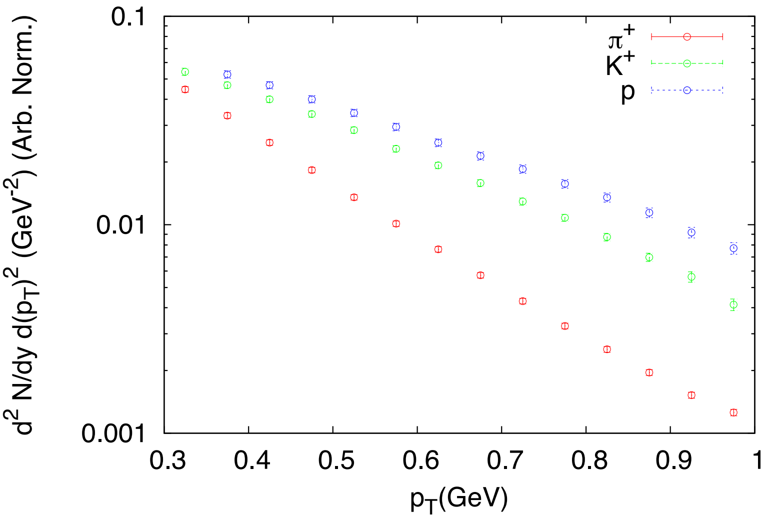

Figure 1.3: Transverse momentum distribution of particle yields of different particles at 5.02 TeV in pPb collision.

gluon plasma formation is not expected and the system is too small for hydrodynamics to be applicable.

Leonidov et al.[3] proposed a simple random walk model to explain this mass dependence without assuming any collective behaviour. Low energy studies indicated no strong evidence to discard this model in favour of models including collectivity[4]. In this thesis, the effectiveness of the random walk model to describe the transverse momentum distribution of particle yields is studied using newly available data at higher energies at the Relativistic Heavy Ion Collider and the Large Hadron Collider. It is then compared with the blast wave model proposed by Schnedermann et al.[5], perhaps the simplest model which includes collectivity.

In Chapter 2, we discuss how the results from the random walk model explains the mass dependence of the slope of transverse momentum distribution of hadrons in p+Pb collisions but fails miserably for Pb+Pb collisions. The results from blast wave model in turn explains experimental observation in Pb+Pb collisions. After considering the effectiveness of the random walk model, which does not include collectivity, and comparing it to the phenomenological, hydrodynamics inspired blast wave model, attention is directed to true hydrodynamic calculation. The typical Navier-Stokes equations used in case of non-relativistic fluids is inadequate in case of the relativistic scenario encountered here, so the appropriate formalism is developed.

1.3 Conventions

Since heavy ion collisions of interest to us occur at relativistic energies, it extensively makes use of special relativity. Rather than the usual kinematic variable like four momentum or four velocity, a different convenient set of quantities are popular in collision literature.

Table 1.1: Metric value of quantities in natural unit

Unit	Metric Value
1 eV^{-1} of length	1.97×10^{-7} m
1 eV of mass	1.78×10^{-36} kg
1 eV^{-1} of time	6.58×10^{-16} s
1 eV of temperature	1.16×10^{4} K

All quantities are expressed in natural units, with $c = \hbar = k_B = 1$. Hence, the unit of energy, momentum, mass and temperature is GeV. Length and time has the unit GeV^{-1}.

Energy is usually reported in the centre of mass frame as $\sqrt{s}$, in terms of the Mandelstam variable $s = (p_1 + p_2)^2$, where p_1 and p_2 are the four momenta of the colliding particles. Energy is sometimes also reported in the laboratory frame, in which case the unit is written as AGeV or GeV/n, where A is the mass number and "/n" represents per nucleon. One can express s in terms of the laboratory frame energy E^* as

$$s = m_{pro}^2 + m_{tar}^2 + 2m_{tar}E^*$$

where m_{pro} is the mass of the projectile and m_{tar} is the mass of the target.

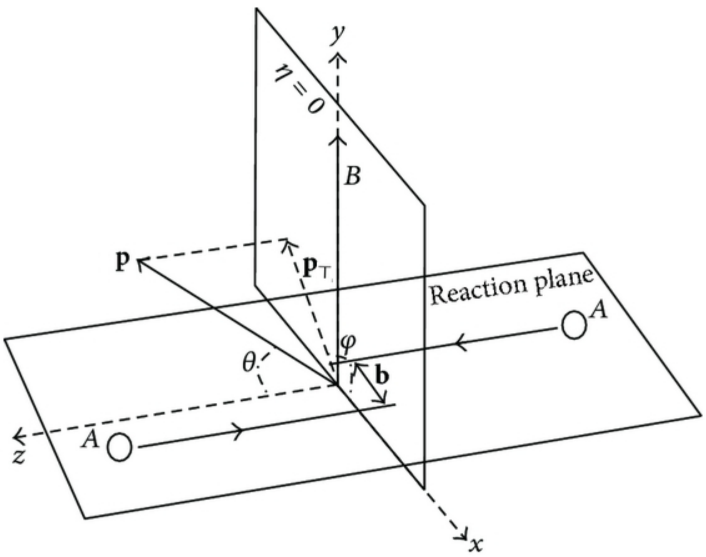

Figure 1.4: Center-of-mass scattering angle.[6]

By convention, z-axis is taken to be parallel to the particle beam. Since the collision does not need to be central in general, the x-axis is taken in the direction of the impact vector. The azimuthal angle is defined with respect to the x-axis.

Transverse momentum p_T is the projection of momentum on the x-y plane. *Transverse mass* m_T is defined as $\sqrt{p_T^2 + m^2}$.

Rapidity y is defined as $\frac{1}{2}\ln\left(\frac{E+p_z}{E-p_z}\right)$, where E is the zeroth component of the four momentum of the particle, which is its energy, and p_z is the third or z component of the particle momentum. Rapidity is additive, unlike velocity, under Lorentz transformation. That is, if a particle has rapidity y_1 in frame 1 and frame 1 has rapidity y_2 in frame 2, the rapidity of the particle in frame 2 is simply $y_1 + y_2$. It is also worth noting that $p_0 = m_T \cosh y$ and $p_z = m_T \sinh y$.

Pseudo-rapidity is defined as $-\ln\tan(\theta/2)$, where θ is the centre-of-mass scattering angle, as shown in Figure 1.4.

Chapter 2

Random-walk model

2.1 The Model

The random-walk model aims to give a schematic description of the collision of nuclei at high energy without assuming any sort of collective behaviour[3]. It assumes that the collision of two nucleons gives rise to a thermal system, called "fireball", which decays without interacting any further. In each successive interaction of a nuclear collision, a fireball just like that formed in a nucleon-nucleon collision is formed. If a nucleon starts with zero p_T , after the first collision, the next one will generally occur at some non-vanishing transverse velocity. Thus there is a gain in transverse momentum through successive collisions. The propagation of the nucleon through successive collisions in the target is assumed to follow a random walk pattern. A process involving a large number of nucleons is simply treated as the superposition of individual collisions between the projectile and the target nuclei.

According to elementary statistical mechanics, the momentum distribution of hadrons emitted by a fireball at temperature T is given by

$$\frac{d^3N}{d^3\vec{p}} = \frac{V_0}{(2\pi)^3} \exp\left(-p_0/T\right)$$

where $p_0 = \sqrt{\vec{p}^2 + m^2}$ is the energy of the emitted hadron and V_0 is the volume of the fireball. In terms of longitudinal rapidity y, transverse mass m_T and azimuthal angle ϕ, the above equation becomes

$$\frac{d^3N_0}{dydp_T^2d\phi} = \frac{V_0 m_T}{2(2\pi)^3} \cosh y \exp\left\{-(m_T \cosh y)/T\right\} \tag{2.1}$$

The fireballs to be superimposed will not, in general, be at rest. Hence, we need the analogue of Equation (2.1) in a boosted frame. The velocity of this boosted frame can be expressed in terms of cylindrical coordinates with respect to the collision centre of mass, relative to the initial collision axis. If ρ denotes the transverse rapidity, Y the longitudinal rapidity and Φ the azimuthal orientation of a fireball, its Boltzmann factor would be given by[7]

$$\exp\{-p_\mu u^\mu/T\} = \exp\{-[m_T \cosh\rho \cosh(Y-y) - p_T \sinh\rho \cos(\Phi-\phi)]/T\}$$

Using this, the analogue of Equation (2.1) arising due to fireball superposition turns out to be

$$\frac{d^3N}{dydp_T^2d\phi} = \frac{V_0 m_T}{2(2\pi)^3}\iiint d\rho\, dY\, d\Phi\ f(\rho, Y, \Phi)\cosh(Y-y)\exp\{-p_\mu u^\mu/T\}$$

where $f(\rho, Y, \Phi)$ denotes the kinematic distribution of the fireball. Performing the Φ integral assuming azimuthal symmetry,

$$\frac{d^2N}{dydp_T^2} = \frac{V_0 m_T}{2(2\pi)^3}\int d\rho\ I_0(p_T \sinh\rho/T) \int dY\ f(\rho, Y)\cosh(Y-y)\exp\{-m_T\cosh(Y-y)\cosh\rho/T\} \quad (2.2)$$

In our analysis, we will be looking at particles at a rapidity range close to zero, hence we may put $y = 0$ in the above equation. The rapidity possible in the fireball, denoted by Y, would be limited by the rapidity the incident nucleon can impart on it. At a given beam energy, the maximum possible rapidity the projectile could impart would be for a head on elastic collision by a nucleon travelling along the z-axis. This turns out to be approximately given by

$$y_{in} = \ln(\sqrt{s}/M)$$

where M is the mass of the nucleon. We may put a cutoff on Y as given by

$$Y_L \approx y_{in} - \coth y_{in} + \frac{1}{\sinh y_{in}}$$

The kinematic distribution of the fireball is assumed to be independent of the longitudinal rapidity Y as suggested by Bjorken[8]. Now the kinematic distribution of the fireball is only a function of ρ, except for a cutoff at some $\pm Y_L$,

The path of the incident nucleon is considered to be a random walk through the target in this model. Hence, the kinematic distribution of the fireballs in a p-A collision, as a function of transverse rapidity, will follow a Gaussian as given by

$$f_{pA}(\rho) = \left[\frac{4}{\pi\delta_{pA}^2}\right]^{1/2} \exp\left(-\rho^2/\delta_{pA}^2\right)$$

where δ_{pA} is related to the average transverse rapidity shift per collision δ as

$$\delta_{pA}^2 = (N_A - 1)\delta^2$$

where N_A is the number of nucleons the incident proton encounters during its journey.

In nucleus-nucleus collision, scattering of both the target and projectile will occur. The gaussian form remains the same, but δ_{pA} must be replaced by δ_{AA} given by

$$\delta_{AA}^2 = (N_A + N_B - 2)\delta^2$$

Note that, for a large nuclei, $N_A \approx 0.57A^{1/3}$, from Glauber model[9].

Substituting $f(\rho, Y)$ in Equation (2.2) in accordance with the above reasoning,

$$\left(\frac{d^2N}{dydp_T^2}\right)_{y=0}^{pA} = \frac{V_0 m_T}{2(2\pi)^3}\left[\frac{4}{\pi\delta_{pA}^2}\right]^{1/2}\int_0^\infty d\rho\ \exp\left(-\rho^2/\delta_{pA}^2\right) I_0(p_T \sinh\rho/T)$$
$$\int_{-Y_L}^{Y_L} dY\ \cosh Y \exp\left\{-m_T \cosh Y \cosh\rho/T\right\} \quad (2.3)$$

In a p-p collission, there will not be any transverse rapidity, so $\delta \to 0$. The resulting Dirac delta will remove the ρ integral. At high energy, Y_L becomes sufficiently large to include the most of the contribution from the integrand, so we may replace it in the limits by ∞. Now, applying $K_1(z) = \int_0^\infty \cosh y e^{-z\cosh y} dy$,

$$\left(\frac{d^3N_0}{dydp_T^2}\right)^{pp} \approx const. m_T K_1(m_T/T) \quad (2.4)$$

2.2 Analysis

The model contains two free parameters, T and δ, if the normalisation factors in the equations are not counted. Since the model assumes the absence of collective behaviour, the following methodology was adopted to verify the effectiveness of the model. T could be extracted for a particular particle at a particular energy from p-p collision data using Equation (2.4). Once T was known for a particular particle and energy, δ could obtained for the same using Equation (2.3) from p-A collision data. Once both of these parameters were known, the prediction of the model for A-A collision could be computed, since the model treats an A-A collision merely as a superposition of p-A-like events.

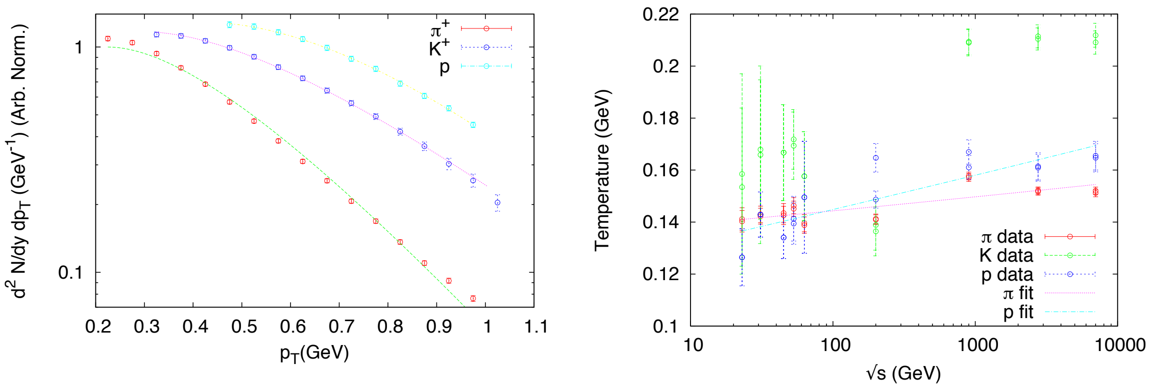

(a) Particle yield as a function of transverse momentum for various particles at 2.76 TeV. The data is fitted with Equation (2.4).

(b) Summary of T obatined for varous particles at various energies. The error bars represent 95% confidene interval.

Figure 2.1

As outlined above, the first step was to obtain T. Particle yields of $\pi^{\pm}, K^{\pm}, p$ and $\bar{p}$ in p-p collisions was available for various energies ranging from 23 GeV to 7 TeV. The particle yields were fitted with Equation (2.4), keeping the normalisation factor and T as parameters. A sample fit is shown in Figure 2.1a and the complete set of fits are attached in Appendix A. The value of T obtained for all the particles over the whole energy range is summarised in Figure 2.1b. T for $\pi^{\pm}, p$ and $\bar{p}$ were found not to change much over a large energy range hence their average values, 145 MeV for $\pi^{\pm}$ and 150 MeV for p and $\bar{p}$, were used in subsequent calculations. No such average could be used in case of $K^{\pm}$.

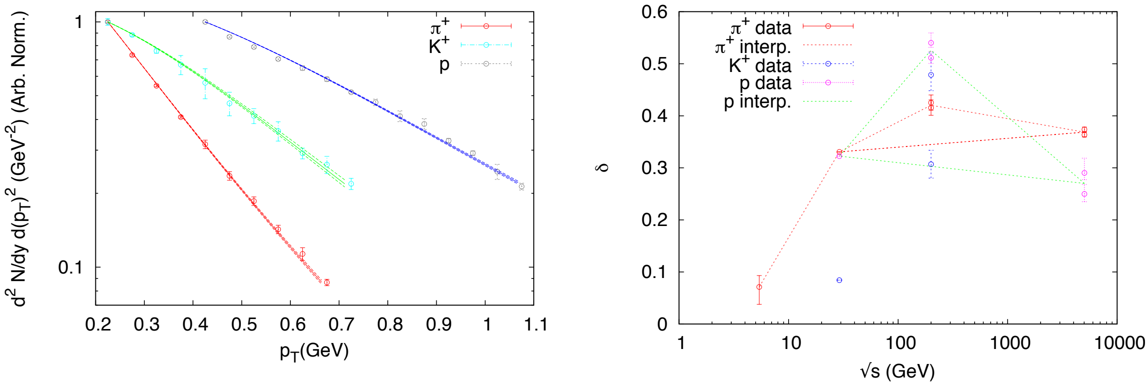

(a) Particle yield as a function of transverse momentum for various particles in d-Au colission at 200 GeV. The data is fitted with Equation (2.3). The dotted lines at either side of the fitted curve denotes the 1-σ variation.

(b) Summary of δ obatined for varous particles at various energies. The error bars represent 1-σ interval. Various interpolating lines are also shown.

Figure 2.2

Once T was obtained, p-A collision data was used to obtain δ. Collisions of protons with various nuclei like Pb, Au, Cu, Al and Be were available. The available collision data of deuterium with Au was also used, assuming the small size of deuterium would make it unlikely to contribute to collectivity dramatically, if it existed. In hindsight, δ values obtained from collisions with Pb and Au (having similar number of nucleons as Pb) were only used. A sample fit is shown in Figure 2.2a and the complete set of fits are attached in Appendix B. The value of δ obtained over the whole energy range is summarised in Figure 2.2b. The interpolated values of δ could be used over the whole energy range. Fit for $K^{\pm}$ at 5.02 TeV was converging at $\delta \to 0$, so inclusion of $K^{\pm}$ in further analysis became unfeasible. *This exercise led to an important conclusion that the random walk model is able to explain the mass dependence of the slope of* *momentum distribution of hadrons produced in p-A collisions.*

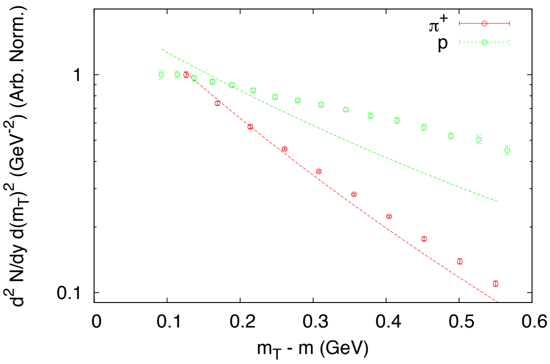

(a) Particle yield as a function of transverse mass for various particles in Au-Au collission at 200 GeV. The yield predicted by random walk model is superimposed

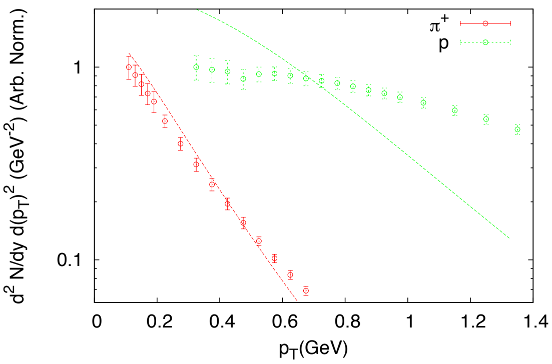

(b) Particle yield as a function of transverse momentum for various particles in Pb-Pb collision at 2.760 TeV. The yield predicted by random walk model is superimposed

Figure 2.3

After obtaining both T and δ, the yield for A-A collisions could be predicted. Data of Pb-Pb and Au-Au collisions at various energies was used for comparison. Figure 2.3 shows data superimposed with the predicted curve for a 200 GeV collision and a 2.76 TeV collision. The complete set of fits are attached in Appendix C. It is clear that the predicted curve does not agree well with the data at higher energies. One can also notice less deviation at lower energy and for lower mass particle. *This indicates that there is additional physics, beyond what is accounted for in random walk model, in A-A collision.*

2.3 An Alternative Including Collectivity - Blast Wave Model

The blast wave model is a model inspired by hydrodynamics, though it is heavily simplified and does not actually solve any hydrodynamic equations[5].

The colliding nuclei are assumed to form a mass of transverse radius R and transverse velocity distribution $\beta(r) = \beta_s \left(\frac{r}{R}\right)^n$. $n = 2$ closely resembles hydrodynamics, which is what motivated this choice. The boost angle $\rho = \tanh^{-1}\beta$ is used to define a transverse velocity field using $\beta(r)$.

$$u'(t, \vec{r}, z = 0) = (\cosh\rho, \hat{r}\sinh\rho, 0)$$

Now, this field is boosted in the longitudinal direction by boost angle η to generate the whole velocity field.

$$u = (\cosh\rho\cosh\eta, \hat{r}\sinh\rho, \cosh\rho\sinh\eta)$$

For a general current j^μ describing the flow of some density like particle number, the amount passing through a surface element $d\sigma_\mu$ is given by $j^\mu d\sigma_\mu$, where $d\sigma_\mu$ is of the form[10] $d\sigma = (d^3\vec{x}, dt\vec{dS})$. $j^0 d^3\vec{x}$ counts the number of particles in the entire spatial volume traversed by the spatial part of the surface in time dt and $-dt\vec{j}.\vec{dS}$ accounts for the flow of the particles in and out of this volume during this time interval. The invariant momentum spectrum of particles emitted from a four surface σ in the velocity field u at temperature T would then be given by

$$\frac{d^3N}{d^3\vec{p}/E} \approx C \int_\sigma e^{-(u^\nu p_\nu - \mu)/T} p^\mu d\sigma_\mu$$

where Boltzmann distribution is used as an approximation and C is a constant.

We now parameterize this surface using coordinates r, ϕ and ζ (we require three parameters since it is the surface in a four dimensional space). For simplicity, we assume the form

$$\sigma(r, \phi, \zeta) = (t(\zeta), r\cos\phi, r\sin\phi, z(\zeta)) \qquad 0 \le r \le R,\ 0 \le \phi < 2\pi,\ |\zeta| \le \eta_{max}$$

At any instant of time $t(\zeta)$, this is a disc of radius R parallel to the x-y plane, with its position along the z-axis given by $z(\zeta)$. The surface element is given by the definition

$d\sigma = (d^3\vec{x}, dtd\vec{S})$ as

$$d\sigma = (rdrd\phi dz, 0, 0, dtrdrd\phi)$$

If we denote $p = (m_T \cosh y, \vec{p}_T, m_T \sinh y)$

$$u^\mu p_\mu = m_T \cosh(y - \eta) \cosh \rho - p_T \sinh \rho \cos(\Delta\phi)$$

where $\Delta\phi$ is the angle between $\hat{r}$ and $\vec{p}_T$. Also,

$$p^\mu d\sigma_\mu = \left(m_T \cosh y \frac{\partial z}{\partial \zeta} - m_T \sinh y \frac{\partial t}{\partial \zeta} \right) rdrd\phi d\zeta$$

$$E\frac{d^3N}{d^3p} = \frac{d^3N}{dyd^2\vec{p}_T} = C \int_{-\eta_{max}}^{\eta_{max}} d\zeta \left(m_T \cosh y \frac{\partial z}{\partial \zeta} - m_T \sinh y \frac{\partial t}{\partial \zeta} \right)$$
$$\int_0^R rdr \exp\left(-\frac{m_T \cosh(y-\eta)\cosh\rho - \mu}{T} \right) \int_0^{2\pi} d\phi \exp\left(\frac{p_T \sinh\rho \cos(\Delta\phi)}{T} \right)$$

Since there is azimuthal symmetry, we can perform the $\Delta\phi$ integral using $I_0(z) = \frac{1}{2\pi}\int_0^{2\pi} e^{z\cos\phi} d\phi$

$$\frac{d^3N}{dyd^2\vec{p}_T} = 2\pi C \int_{-\eta_{max}}^{\eta_{max}} d\zeta \left(m_T \cosh y \frac{\partial z}{\partial \zeta} - m_T \sinh y \frac{\partial t}{\partial \zeta} \right)$$
$$\int_0^R rdr \exp\left(-\frac{m_T \cosh(y-\eta)\cosh\rho - \mu}{T} \right) I_0\left(\frac{p_T \sinh\rho}{T} \right)$$

Since we will be looking at particles at a rapidity range close to zero in our analysis, we may put y = 0 in the above equation. Thus, the above equation reduces to

$$\frac{d^3N}{dyd^2\vec{p}_T} \propto m_T \int_0^R rdrK_1\left(\frac{m_T \cosh\rho}{T} \right) I_0\left(\frac{p_T \sinh\rho}{T} \right) \tag{2.5}$$

In the blast wave model, the effective temperature of the system has contributions arising from two sources - one due to randomness and one due to collective flow, parameterised by T and β_s respectively.

Equation (2.5) was used to fit all available A-A data. The data was seen to fit well through the whole energy range ($\sqrt{s} \approx 9$ GeV to $\sqrt{s} = 2.76$ TeV) . A sample fit is

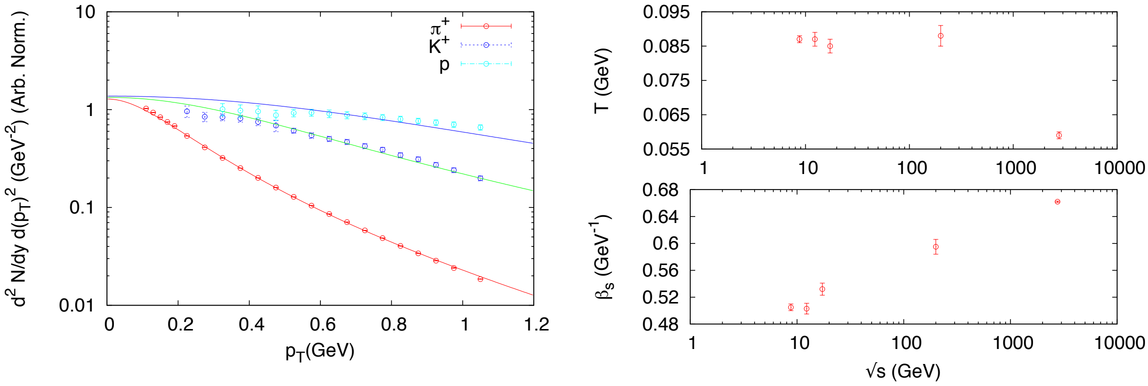

(a) Particle yield as a function of transverse momentum for various particles in Pb-Pb collision at 2.760 TeV. The fit of blast wave model Equation (2.5) is superimposed.

(b) Summary of parameter values obtained at various energies. The error bars represent 1-σ interval. Note the increasing trend in β_s and the decreasing trend in T.

Figure 2.4

shown in Figure 2.4a (Appendix D contains all the fits) and the values of parameters T and β_s obtained over the whole energy range is summarised in Figure 2.4b. A system at higher energy would evolve for more time before freeze out. Naively, one would expect this to result in larger β_s, since there would be more time for collectivity to develop. The freeze out temperature T would be expected to be lower at higher energy, since longer time before freeze out would result in a cooler system. The observed trend in the parameter values conform to this expectation.

2.4 Conclusion

Mass dependence of the slope of transverse momentum distribution of particle yields, as shown in Figure 1.2, supported the expectation that hydrodynamics is at work during heavy ion collision. However, similar feature in p-A collisions, as shown in Figure 1.3, where the system in too small for hydrodynamics to be justified, warrants explaining this mass dependence using some physics other than hydrodynamics. The random walk model was a possible candidate for this. Studies so far at lower energies have been unable to discard random walk model in favour of models including collectivity[4].

In our study also, at all available energies, the *random walk model is seen to explain the mass dependence of the slope in p-A collisions* remarkably well. However, as shown in Figure 2.3, the *random walk model is seen to be inadequate to explain heavy ion collisions* at high energy. The deviation of random walk model from experimental data is also seen to be more dramatic for the heavier of the two particles, which further suggests unaccounted collective behaviour, since heavier particles are expected to show more collective energy ($\propto m\beta^2$). The blast wave model, which is perhaps the simplest model including collectivity, is seen to fit the data quite well, even at higher energies.

Irrespective of its effectiveness, the blast wave model is a phenomenological model and says nothing about many aspects of the system which are of interest, like the evolution of the system. Since there is strong reason to believe that collective behaviour is present, it would be appropriate to pursue the more physically sound hydrodynamic formulation from which the blast wave model draws its inspiration. We direct our attention to a hydrodynamic formulation of heavy ion collisions in the subsequent chapters.

Chapter 3

Hydrodynamics in Relativistic Heavy Ion Collsion

Hydrodynamics is the discipline which studies liquids in motion. It is useful for understanding a wide range of phenomenon, ranging from galactic evolution[11] to insect flight[12].

In hydrodynamics, the fluid is assumed to be a continuum—the particulate nature of the constituents are ignored and quantities like density, pressure, temperature, and velocity are defined by continuous fields. The main pillars of hydrodynamics are the conservation laws, specifically, conservation of mass, momentum and energy.

For fluids which are sufficiently dense to be a continuum, do not contain charged particles, and have velocities small in relation to the speed of light, the Navier-Stokes equations are the relevant hydrodynamical equations. It describes the flow of a non-relativistic fluid whose stress depends linearly on velocity gradients and pressure. In an inertial frame of reference, it is given by

$$\rho\left(\frac{\partial \vec{v}}{\partial t} + (\vec{v}.\nabla)\vec{v}\right) = -\nabla p + \nabla.\mathcal{T} + \vec{f}$$

where $\vec{v}$ is the flow velocity, ρ is the fluid density, p is the pressure, $\mathcal{T}$ is the deviatoric component of the stress tensor (order two), and $\vec{f}$ represents the forces per unit volume acting on the fluid.

Heavy ion collisions occur at relativistic speeds. Hence, the familiar Navier-Stokes equations are not applicable in their case. One needs to apply the conservation laws in a relativistic setting to derive the relevant equations. Before we proceed to the derivation, let us direct our attention once again to the different stages of evolution after the collision of two heavy ions, with a view of understanding where hydrodynamics is applicable.

3.1 Spacetime Evolution in Heavy Ion Collisions

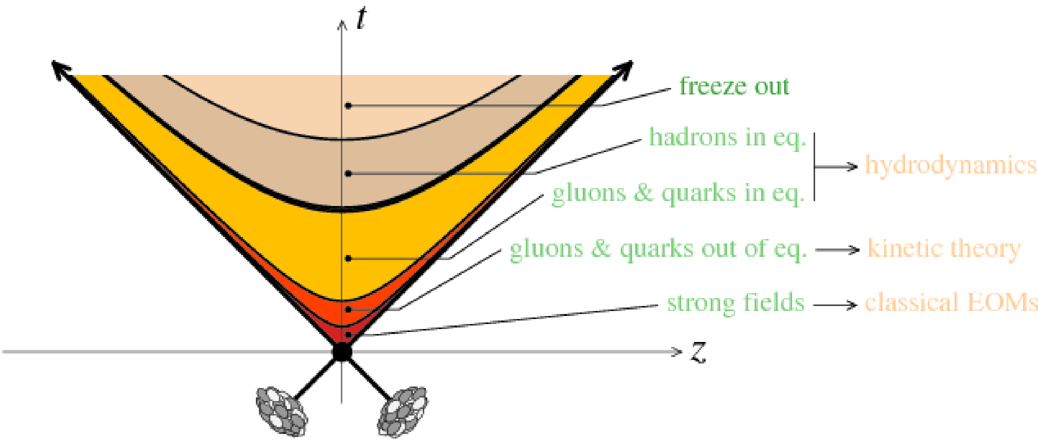

Figure 3.1: Diagram depicting spacetime evolution of heavy ion collision.[13]

The different stages of heavy ion collision can be broadly divided into the following categories:

- Initial Stage : Two nuclei approach each other with relativistic speed. Because of their high speed, the colliding nuclei are highly Lorentz contracted into pancake-like shapes. The collision is conventionally said to occur at time $t = 0$.
- Pre-equilibrium stage : After collision, a large amount of the initial kinetic energy of the incoming nucleons are deposited into a very small region. Strong interaction between quarks and gluons of the colliding nucleons helps to achieve local thermal equilibrium quickly at around $t \approx 1$ fm.
- QGP evolution : The space-time evolution of the QGP can be described by relativistic hydrodynamics, since local thermal equilibrium is already achieved.

When the temperature of the QGP drops below a critical value, quarks and gluons form colourless hadrons.

- Hadron gas and freeze out : The hadron gas expands and cools down obeying relativistic hydrodynamics, until the mean free path of the constituent hadrons becomes large compared to the system size. When this happen, hadrons no longer interact and their momentum distribution remains unchanged thereafter, causing *kinetic freezeout.* Before kinetic freeze out, there is a stage when inelastic collisions stop, fixing the number of particles of different kind, called *chemical freezeout.*

Hydrodynamics is believed to be applicable from the thermalisation until kinetic freeze out. The typical time duration is of the order of $\sim 10-15$ fm. It must be noted that in experiments, we only observe the hadronic residue of the collision, along with photons and leptons, and all the other information has to be inferred from it.

3.2 Relativistic Hydrodynamics

In the previous section, we discussed that a major portion of the space-time evolution during heavy ion collisions can be described using relativistic hydrodynamics. One of the first application of relativistic hydrodynamics in high energy nuclear collisions was done by Landau.[14] According to Landau, the motivations behind the applicability of hydrodynamics are the following:

- Due to high velocity, the accelerating nucleus becomes highly Lorentz contracted. After collision, a large amount of energy is deposited in a small volume by the inelastic collisions between the nucleons and large number of particles are formed. The mean free path in the resulting system is small compared to the whole volume and statistical equilibrium sets up.

- In the next stage, the expansion of the system is described by hydrodynamic equations. During the process of expansion, the mean free path remains small in comparison to system size, and this justify the use of hydrodynamics. Since the velocities in the system is comparable to the speed of light, we must use relativistic hydrodynamics.

- As the system expands, the interaction becomes weaker and mean free paths becomes longer. The number of particles appears as a physical characteristic when the interaction becomes sufficiently weak. When the mean free path becomes comparable to the linear dimension of the system, the latter breaks up into particles. This was called as "break-up" stage. The break-up occurs when the temperature of the system becomes comparable to the pion mass.

At very high energy, J.D. Bjorken[8], proposed a modification to Landaus hydrodynamic model. According to Bjorken, at very high energy, the colliding nucleons becomes transparent. Essentially, the system continues with the same velocity it had just before collision just after the collision also. Particle productions per unit rapidity only depends on the initial energy density. The entropy per unit rapidity is conserved, as a consequence of the boost symmetry.

Now we direct our attention to deriving the hydrodynamic equations. A perfect or ideal fluid is defined to be that which obeys Pascals law and is incapable of supporting any shear force applied to it. By utilising the physical identification of the components of the energy-momentum tensor[15], the energy-momentum tensor of an isotropic and perfect fluid in its local rest frame turns out to be

$$T_R^{\mu\nu} = \begin{pmatrix} \epsilon & 0 & 0 & 0 \\ 0 & P & 0 & 0 \\ 0 & 0 & P & 0 \\ 0 & 0 & 0 & P \end{pmatrix}$$

where ϵ is the energy density and P is the pressure in the local rest frame of the fluid.

We may obtain the energy-momentum tensor in a general inertial frame by employing the appropriate Lorentz transformation. Consider a Lorentz boost Λ^μ_ν along $u^\mu = (\gamma, \gamma\vec{v})$. If we apply this to the unit velocity in the rest frame $u^\mu_R = (1, \vec{0})$, we get

$$\begin{aligned} u^\mu &= \Lambda^\mu_\nu u^\nu_R \\ \Rightarrow u^\mu &= \Lambda^\mu_0 \end{aligned}$$

We may write the metric in the boosted frame as

$$\begin{aligned} g^{\mu\nu} &= \Lambda^\mu_\sigma \Lambda^\nu_\rho g^{\sigma\rho} \\ &= \Lambda^\mu_0 \Lambda^\nu_0 g^{00} + \Lambda^\mu_i \Lambda^\nu_i g^{ii} \\ \Rightarrow \Lambda^\mu_i \Lambda^\nu_i &= u^\mu u^\nu - g^{\mu\nu} \end{aligned}$$

We now Lorentz transform the energy-momentum tensor $T^{\mu\nu}_R$.

$$\begin{aligned} T^{\mu\nu} &= \Lambda^\mu_\sigma \Lambda^\nu_\rho T^{\sigma\rho}_R \\ &= \Lambda^\mu_0 \Lambda^\nu_0 \epsilon + \Lambda^\mu_i \Lambda^\nu_i P \\ &= u^\mu u^\nu (\epsilon + P) - g^{\mu\nu} P \end{aligned} \tag{3.1}$$

We now invoke the continuity equation for the energy-momentum tensor.

$$\partial_\mu T^{\mu\nu} = 0$$

In the rest frame of the fluid, this yields $\frac{\partial\epsilon}{\partial t} = 0$ and $\frac{\partial P}{\partial x^i} = 0$. However, since we are interested in a moving fluid, we utilise equation (3.1) to obtain

$$\left[(\partial_\mu u^\mu) u^\nu + u^\mu (\partial_\mu u^\nu)\right](\epsilon + P) + u^\mu u^\nu \partial_\mu (\epsilon + P) - g^{\mu\nu} \partial_\mu P = 0 \tag{3.2}$$

We now contract equation (3.2) with u_ν. Using $u_\nu u^\nu = u_{R\nu} u^\nu_R = 1$ and $u_\nu \partial_\mu u^\nu = \frac{1}{2}\partial_\mu (u_\nu u^\nu) = 0$, we obtain

$$(\epsilon + P)\partial_\mu u^\mu + u^\mu \partial_\mu \epsilon = 0 \tag{3.3}$$

Dividing the first law of thermodynamic by volume, one obtains

$$\epsilon + P = Ts + \mu n_{bar} \tag{3.4}$$

where ϵ is the energy density, P the pressure, T the temperature, s the entropy density μ the chemical potential and n_{bar} the baryon density. Fixing P, T and μ in the above equation,

$$\partial_\mu \epsilon = T\partial_\mu s + \mu \partial_\mu n_{bar}$$

Substituting $(\epsilon + P)$ and $\partial_\mu \epsilon$ in equation (3.3) using the above two equations,

$$T\partial_\mu (su^\mu) + \mu \partial_\mu (n_{bar} u^\mu) = 0$$

Here $n_{bar} u^\mu$ is the baryon current and since baryon number is conserved, $\partial_\mu (n_{bar} u^\mu) = 0$. Hence,

$$\partial_\mu (su^\mu) = 0 \tag{3.5}$$

One can use the identity $\partial_\mu \ln s = \frac{1}{c_s^2} \partial_\mu \ln T$, where c_s is the speed of sound in the medium, in the above equation to obtain the first hydrodynamic equation.

$$\boxed{\partial_\mu u^\mu + \frac{1}{c_s^2} u^\mu \partial_\mu \ln T = 0} \tag{3.6}$$

In order to obtain the second hydrodynamic equation, we contract equation (3.2) with $g_{\lambda\nu} - u_\lambda u_\nu$, a tensor orthogonal to u_ν (in the sense $u^\nu [g_{\lambda\nu} - u_\lambda u_\nu] = u_\lambda - u_\lambda = 0$). Again, utilising $u_\nu u^\nu = 1$ and $u_\nu \partial_\mu u^\nu = 0$, we obtain

$$(\epsilon + P) u^\mu \partial_\mu u_\lambda - \partial_\lambda P + u_\lambda u^\mu \partial_\mu P = 0 \tag{3.7}$$

We now keep ϵ, s and n_{bar} fixed in equation (3.4) to obtain

$$\partial_\lambda P = s\partial_\lambda T + n_{bar} \partial_\lambda \mu$$

Replacing $(\epsilon + P)$ and $\partial_\lambda P$ in equation (3.7) using equation (3.4) and the above equation,

$$s[u^\mu \partial_\mu (u_\lambda T) - \partial_\lambda T] + n_{bar}[u^\mu \partial_\mu (u_\lambda \mu) - \partial_\lambda \mu] = 0$$

We utilise $n_{bar} \approx 0$, which holds good in relativistic collisions, to simplify the above equation.

$$u^\mu \partial_\mu (u_\lambda T) - \partial_\lambda T = 0 \tag{3.8}$$

Dividing by T and simplifying, we get the second hydrodynamic equation.

$$\boxed{u^\mu \partial_\mu u_\lambda - \partial_\lambda \ln T + u_\lambda u^\mu \partial_\mu \ln T = 0} \tag{3.9}$$

Chapter 4

Hydrodynamics in 1+1 D

In heavy ion collisions, the expansion of the system after collision in the longitudinal direction is much greater than that in the transverse direction. As a simplification, we may assume the velocity of the fluid in cylindrical coordinates to be

$$u^\mu(t, v_z, v_r \approx 0, v_\phi = 0) = (\cosh\theta, \sinh\theta, 0, 0) \tag{4.1}$$

where θ is the boost angle $\tanh^{-1} v_z$.

4.1 Simplification

Using the above definition for u^μ,

$$u^\mu \partial_\mu = \cosh\theta \frac{\partial}{\partial t} + \sinh\theta \frac{\partial}{\partial z} \tag{4.2}$$

$$\partial_\mu u^\mu = \sinh\theta \frac{\partial \theta}{\partial t} + \cosh\theta \frac{\partial \theta}{\partial z}. \tag{4.3}$$

Substituting these in equations (3.3) and (3.7), we get

$$(\epsilon + P)\left(\sinh\theta \frac{\partial\theta}{\partial t} + \cosh\theta \frac{\partial\theta}{\partial z}\right) + \cosh\theta \frac{\partial\epsilon}{\partial t} + \sinh\theta \frac{\partial\epsilon}{\partial z} = 0 \tag{4.4}$$

$$(\epsilon + P)\left(\cosh\theta \frac{\partial\theta}{\partial t} + \sinh\theta \frac{\partial\theta}{\partial z}\right) + \sinh\theta \frac{\partial P}{\partial t} + \cosh\theta \frac{\partial P}{\partial z} = 0, \tag{4.5}$$

apart from the trivial equations $\partial P/\partial r = 0$ and $\partial P/\partial\phi = 0$.

We replace the cartesian coordinates used in the above equations with light cone variables,

$$y = \frac{1}{2}\ln\left(\frac{t+z}{t-z}\right)$$

$$\tau = \sqrt{t^2 - z^2}.$$

Noting that $\tanh y = z/t$, the inverse parameterisation is

$$z = \tau \sinh y$$
$$t = \tau \cosh y.$$

Under these coordinates, the partial derivatives transform as

$$\begin{aligned}\frac{\partial}{\partial t} &= \frac{\partial y}{\partial t}\frac{\partial}{\partial y} + \frac{\partial \tau}{\partial t}\frac{\partial}{\partial \tau} \\ &= -\frac{1}{\tau}\sinh y \frac{\partial}{\partial y} + \cosh y \frac{\partial}{\partial \tau} \qquad (4.6)\\ \frac{\partial}{\partial z} &= \frac{1}{\tau}\cosh y \frac{\partial}{\partial y} - \sinh y \frac{\partial}{\partial \tau}. \qquad (4.7)\end{aligned}$$

Substituting these in Eq. (4.4) and Eq. (4.5) and using the summation identities for hyperbolic trigonometric functions, followed by multiplication with $\tau/\cosh(\theta - y)$ gives

$$\boxed{(\epsilon + P)\left(\frac{\partial \theta}{\partial y} + \tau \tanh(\theta - y)\frac{\partial \theta}{\partial \tau}\right) + \tanh(\theta - y)\frac{\partial \epsilon}{\partial y} + \tau \frac{\partial \epsilon}{\partial \tau} = 0} \qquad (4.8)$$

$$\boxed{(\epsilon + P)\left(\tanh(\theta - y)\frac{\partial \theta}{\partial y} + \tau \frac{\partial \theta}{\partial \tau}\right) + \frac{\partial P}{\partial y} + \tau \tanh(\theta - y)\frac{\partial P}{\partial \tau} = 0.} \qquad (4.9)$$

Recall the baryon number conservation equation $\partial_\mu(n_{bar}u^\mu) = 0$. Expanding using the definition of u^μ given in Eq. (4.1) gives,

$$n_{bar}\left(\sinh \theta \frac{\partial \theta}{\partial t} + \cosh \theta \frac{\partial \theta}{\partial z}\right) + \cosh \theta \frac{\partial n_{bar}}{\partial t} + \sinh \theta \frac{\partial n_{bar}}{\partial z} = 0.$$

This equation is of the same form as Eq. (4.4), so we can simplify it to

$$\boxed{n_{bar}\left(\frac{\partial \theta}{\partial y} + \tau \tanh(\theta - y)\frac{\partial \theta}{\partial \tau}\right) + \tanh(\theta - y)\frac{\partial n_{bar}}{\partial y} + \tau \frac{\partial n_{bar}}{\partial \tau} = 0.} \qquad (4.10)$$

Equation (4.8), Eq. (4.9) and Eq. (4.10) form a set of three equations in four unknowns, namely ϵ, P, θ and n_{bar}. We require an equation of state, that is, an expression giving pressure P as a function of energy density ϵ, to obtain the solution. For convenience, one looks at c_s^2 where $P = c_s^2\epsilon$. Here, we will proceed with an arbitrary c_s^2, but different types equations of state are discussed in detail in Chapter 5.

4.2 Solution using Bjorken Initial Condition

If the initial system after the ions interact looks the same, regardless of the rapidity, as in the case of Bjorken initial condition, we have

$$\theta(y, \tau_0) = y$$

To use this initial condition in Eq. (4.8), Eq. (4.9) and Eq. (4.10), we start off assuming the following compatible solution for θ

$$\theta(y, \tau) = y.$$

With this, Eq. (4.8), Eq. (4.9) and Eq. (4.10) reduce to

$$\epsilon + P + \tau \frac{\partial \epsilon}{\partial \tau} = 0 \tag{4.11}$$

$$\frac{\partial P}{\partial y} = 0 \tag{4.12}$$

$$n_{bar} + \tau \frac{\partial n_{bar}}{\partial \tau} = 0 \tag{4.13}$$

Equation (4.13) immediately gives

$$\ln \left(\frac{n_{bar}(\tau)}{n_{bar}(\tau_0)} \right) = -\ln \left(\frac{\tau}{\tau_0} \right)$$

Using $P = c_s^2 \epsilon$ in Eq. (4.11), we get

$$\epsilon(1 + c_s^2) + \tau \frac{\partial \epsilon}{\partial \tau} = 0$$

Solving, we get

$$\ln \epsilon \Big|_{\epsilon_i}^{\epsilon_f} = -\int_{\tau_i}^{\tau_f} d\tau \, \frac{(1 + c_s^2)}{\tau}$$

Which finally simplifies to

$$\boxed{\epsilon(\tau_f) = \epsilon(\tau_i) \exp \left[-\int_{\tau_i}^{\tau_f} d\tau \, \frac{(1 + c_s^2)}{\tau} \right]} \tag{4.14}$$

Note that, however, c_s^2 is usually obtained as a function of temperature. To write it as a function of τ, we take Eq. (3.6) and use Eq. (4.2), Eq. (4.3), Eq. (4.6) and Eq. (4.7) to obtain

$$\frac{1}{\tau} + \frac{1}{c_s^2}\frac{\partial \ln T}{\partial \tau} = 0$$

Solving this, we get

$$\frac{\tau_f}{\tau_i} = \exp\left[-\int_{T_i}^{T_f} dT\, \frac{1}{T c_s^2}\right].$$

Inverting the above relation, we can write temperature as a function of τ, which will then enable us to write c_s^2 as a function of τ.

4.3 Results

As mentioned before, we require an equation of state to solve the hydrodynamic equations. The input of the equation of state comes into Eq. (4.14) through c_s^2. In Chapter 5, various types of c_s^2 are discussed in detail.

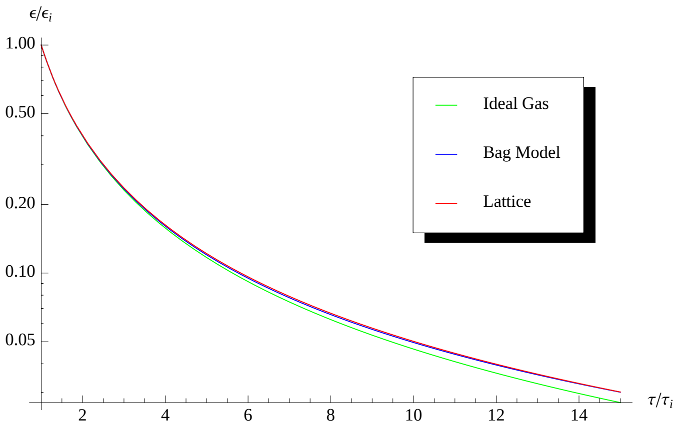

Figure 4.1: Energy density as a function of time for different equations of state.

The simplest type of equation of state one can think of is that of an ideal gas. Though this might be unrealistic, for comparison we have included the ideal gas equation of state. c_s^2 in this case assumes the constant value $\frac{1}{3}$, which is the highest in our range of interest. More realistic values of c_s^2, obtained from the MIT Bag Model and Lattice QCD calculations, are given in Figure 5.5 and Figure 5.6 respectively. The energy density of the heavy ions after collision is plotted as a function of time for various equations of state in Figure 4.1. It is interesting to note that the energy density decreases fastest in case of the ideal gas equation of state. Interpreting c_s^2 as the maximum speed of sound in the medium, this is what one would expect.

Chapter 5

Equations of State

In order to solve the hydrodynamic equations given in the previous section, one needs to have an equation of state. For our purpose, an equation of state is a relation between the pressure P of the system and energy density ϵ. For convenience, we look at the speed of sound c_s, which relates the above quantities as

$$P = c_s^2 \epsilon$$

5.1 Ideal Gas

General equipartition theorem gives the following relation[16] between the Hamiltonian H of a system and the generalised coordinate p:

$$\left\langle p \frac{\partial H}{\partial p} \right\rangle = k_B T.$$

The average is an ensemble average in a microcanonical or a canonical ensamble.

In case of a relativistic ideal gas, the Hamiltonian of a particle is given by

$$H = c\sqrt{p_x^2 + p_y^2 + p_z^2}$$

$$p_i \frac{\partial H}{\partial p_i} = c \frac{p_i^2}{\sqrt{p_x^2 + p_y^2 + p_z^2}}$$

$$\Rightarrow H = p_x \frac{\partial H}{\partial p_x} + p_y \frac{\partial H}{\partial p_y} + p_z \frac{\partial H}{\partial p_z}$$

Applying the equipartition theorem,

$$\langle H \rangle = 3 k_B T$$

The ideal gas equation gives

$$PV = Nk_BT$$

Comparing the above two, we obtain

$$P = \frac{1}{3}\frac{N\langle H\rangle}{V} = \frac{1}{3}\epsilon$$

Recall $P = c_s^2\epsilon$. Hence, in case of an ideal gas,

$$\boxed{c_s^2 = \frac{1}{3}}$$

5.2 Bag Model

It is well known from elementary statistical mechanics[17] that the distribution function and grand partition function (considering only one energy state) for fermions and bosons are given by

$$f(T, E, \mu) = \frac{1}{\exp[(E-\mu)/T] \pm 1}$$

and

$$Z_E = (1 \pm \exp[-(E-\mu)/T])^{\pm 1}$$

respectively, where $+$ is for fermions and $-$ is for bosons. We obtain the same for antiparticles in both cases by changing the sign of the chemical potential.

The generalised $\ln Z$ for particles and antiparticles, either bosons or fermions, is given by

$$\ln Z(T, \mu, V) = \frac{gV}{2\pi^2 T}\int_0^\infty \frac{dkk^4}{3E}\;[f(T, E, \mu) + f(T, E, -\mu)] \tag{5.1}$$

where $+$ is for fermions and $-$ is for bosons. This equation can be obtained from the above Z_E by integrating over all space and momentum coordinates, while changing the variable of integration from k to E and performing an integration-by-parts.

Once the partition function of a system is known, all thermodynamic quantities in the preview of that ensemble can be derived from it. The following relation are also well known:

$$P = \left(\frac{\partial T \ln Z}{\partial V}\right)_{T,\mu} \tag{5.2}$$

$$\epsilon = \frac{T^2}{V}\left(\frac{\partial \ln Z}{\partial T}\right)_{\mu,V} + \mu\frac{T}{V}\left(\frac{\partial \ln Z}{\partial \mu}\right)_{T,V} \tag{5.3}$$

5.2.1 The QGP Phase

The QGP phase is composed of quarks, which are fermions, and gluons, which are bosons. Since the QGP phase is considered to be dominated by the lighter quarks, we may safely assume that in this phase, the quarks and gluons are massless.

We will first direct our attention to gluons, which are considered to be massless bosons.[18] We take $\mu = 0$, since there is no restriction on the boson number. In this case, Eq. (5.1) reduces to

$$T \ln Z_{gluon} = \frac{g_g V}{6\pi^2}\int_0^\infty dk k^3 \frac{1}{\exp\left(k/T\right) - 1}$$

Putting $y = k/T$,

$$\begin{aligned}
T \ln Z_{gluon} &= \frac{g_g V}{6\pi^2} T^4 \int_0^\infty dy y^3 \; \frac{1}{\exp\left(y\right) - 1} \\
&= \frac{g_g V}{6\pi^2} T^4 \int_0^\infty dy y^3 \; \frac{\exp(-y)}{1 - \exp(-y)} \\
&= \frac{g_g V}{6\pi^2} T^4 \int_0^\infty dy y^3 \; \exp(-y)[1 + \exp(-y) + \exp(-2y) + \dots] \\
&= \frac{g_g V}{6\pi^2} T^4 \sum_{n=0}^{\infty} \int_0^\infty dy y^3 \; \exp[-(n+1)y] \\
&= \frac{g_g V}{6\pi^2} T^4 \sum_{n=0}^{\infty} \frac{1}{(n+1)^4} \int_0^\infty d((n+1)y)((n+1)y)^{(4-1)} \; \exp[-((n+1)y)] \\
&= \frac{g_g V}{6\pi^2} T^4 \zeta(4)\Gamma(4),
\end{aligned}$$

where $\zeta(x) = \sum_{n=1}^{\infty} \frac{1}{n^x}$ is the Riemann zeta function. Using $\zeta(4) = \frac{\pi^4}{90}$, we get

$$T \ln Z_{gluon} = \frac{g_g V}{90} \pi^2 T^4. \tag{5.4}$$

Now we direct our attention to quarks, which are considered to be massless fermions.[18] It must be noted that being fermions, we cannot take $\mu_{quark} = 0$. However, $\mu_q = \mu_{\bar{q}}$. Equation (5.1) gives,

$$T \ln Z_{quark} = \frac{g_q V}{6\pi^2} \int_0^\infty dk k^3 \left[\frac{1}{\exp\left[(k - \mu_q)/T\right] + 1} + \frac{1}{\exp\left[(k + \mu_q)/T\right] + 1} \right].$$

The integral over the quark part may be rewritten as

$$\int_0^\infty dk k^3 \frac{1}{\exp\left[(k - \mu_q)/T\right] + 1} = T \left[\int_{-\mu_q/T}^0 \frac{dy(\mu_q + yT)^3}{\exp(y) + 1} + \int_0^\infty \frac{dy(\mu_q + yT)^3}{\exp(y) + 1} \right]$$

and the integral over the antiquark part may be rewritten as

$$\int_0^\infty dk k^3 \frac{1}{\exp\left[(k + \mu_q)/T\right] + 1} = T \left[\int_0^\infty \frac{dy(yT - \mu_q)^3}{\exp(y) + 1} - \int_0^{\mu_q/T} \frac{dy(yT - \mu_q)^3}{\exp(y) + 1} \right].$$

Noting that $1/(\exp(y) + 1) = 1 - 1/(\exp(-y) + 1)$, the second term in the above expression becomes

$$\int_0^{\mu_q/T} \frac{dy(yT - \mu_q)^3}{\exp(y) + 1} = \int_0^{\mu_q/T} dy(yT - \mu_q)^3 - \int_0^{\mu_q/T} \frac{dy(yT - \mu_q)^3}{\exp(-y) + 1}.$$

Putting $y = -y$ and substituting in the above equation,

$$\int_0^\infty dk k^3 \frac{1}{\exp\left[(k + \mu_q)/T\right] + 1} =$$
$$T \left[\int_0^\infty \frac{dy(yT - \mu_q)^3}{\exp(y) + 1} + \int_{-\mu_q/T}^0 dy\ (yT + \mu_q)^3 - \int_{-\mu_q/T}^0 \frac{dy(yT + \mu_q)^3}{\exp(y) + 1} \right].$$

Adding the quark and antiquark part,

$$\begin{aligned} T \ln Z_{quark} &= \frac{g_q V}{6\pi^2} T \left[\int_0^\infty dy \frac{(yT + \mu_q)^3 + (yT - \mu_q)^3}{\exp(y) + 1} + \int_{-\mu_q/T}^0 dy\ (yT + \mu_q)^3 \right] \\ &= \frac{g_q V}{6\pi^2} T \left[\int_0^\infty dy \frac{2(yT)^3 + 6yT\mu_q^2}{\exp(y) + 1} + \frac{1}{T} \frac{\mu_q^4}{4} \right]. \end{aligned}$$

Multiplying the numerator and denominator of $1/[\exp(y)+1]$ by $\exp(-y)$ and Taylor expanding, we get

$$\frac{1}{\exp(y)+1} = \sum_{n=0}^{\infty}(-1)^n \exp[-(n+1)y].$$

$$\begin{aligned}\int_0^{\infty} dy \frac{2(yT)^3}{\exp(y)+1} &= 2T^3 \sum_{n=0}^{\infty}(-1)^n \int_0^{\infty} dy\, y^3 \exp[-(n+1)y] \\ &= 2T^3 \sum_{n=0}^{\infty}(-1)^n \frac{\Gamma(4)}{(n+1)^4}\end{aligned}$$

Now, we use $\sum_{n=0}^{\infty}(-1)^n \frac{1}{(n+1)^x} = \left(1-\frac{2}{2^x}\right)\zeta(x)$ in the above expression. Recalling $\zeta(4) = \frac{\pi^4}{90}$, we get

$$\int_0^{\infty} dy \frac{2(yT)^3}{\exp(y)+1} = 2T^3\Gamma(4)\frac{7}{8}\zeta(4) = \frac{7}{60}\pi^4 T^3.$$

Similarly

$$\int_0^{\infty} dy \frac{6yT\mu_q^2}{\exp(y)+1} = 6T\mu_q^2\Gamma(2)\frac{1}{2}\zeta(2) = \frac{\pi^2}{2}\mu_q^2 T.$$

Putting it all together,

$$T \ln Z_{quark} = g_q V \left[\frac{7\pi^2}{360}T^4 + \frac{\mu_q^2}{12}T^2 + \frac{\mu_q^4}{24\pi^2}\right]. \tag{5.5}$$

The total partition function for the QGP phase is obtained by adding Eq. (5.4) and Eq. (5.5).

$$T \ln Z_{QGP} = V \left[\pi^2\left(\frac{g_g}{90} + \frac{7g_q}{360}\right)T^4 + \frac{\mu_q^2 g_q}{12}T^2 + \frac{\mu_q^4 g_q}{24\pi^2}\right] \tag{5.6}$$

Now, we may use Eq. (5.2) and Eq. (5.3) to compute the pressure and energy density in the QGP phase, which are plotted in Figure 5.1.

$$P_{QGP} = \pi^2\left(\frac{g_g}{90} + \frac{7g_q}{360}\right)T^4 + \frac{\mu_q^2 g_q}{12}T^2 + \frac{\mu_q^4 g_q}{24\pi^2}$$

$$\epsilon_{QGP} = \pi^2\left(\frac{g_g}{30} + \frac{7g_q}{120}\right)T^4 + \frac{\mu_q^2 g_q}{4}T^2 + \frac{\mu_q^4 g_q}{8\pi^2}$$

$$\boxed{\epsilon_{QGP} = 3P_{QGP}}$$

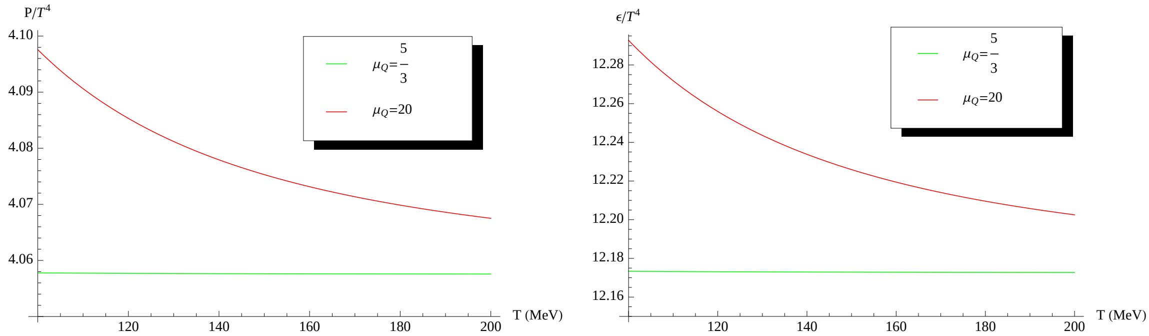

(a) Pressure of QGP as a function of temperature.

(b) Energy density of QGP as a function of temperature.

Figure 5.1: Pressure and Energy density of QGP.

5.2.2 The Hadron Phase

We will first direct our attention to the mesons,[18] which are bosons. Since they have significant mass, we cannot ignore their mass.

$$\begin{aligned}
T \ln Z_{meson} &= \frac{g_m V}{6\pi^2} \int_0^\infty \frac{dk k^4}{\sqrt{k^2+m^2}} \frac{1}{\exp\left(\sqrt{k^2+m^2}/T\right)-1} \\
&= \frac{g_m V}{6\pi^2} T^4 \int_{m/T}^\infty dy \, \left(y^2 - \frac{m^2}{T^2}\right)^{3/2} \frac{1}{\exp\left(y\right)-1} \\
&= \frac{g_m V}{6\pi^2} T^4 \sum_{n=0}^\infty \int_{m/T}^\infty dy \, \left(y^2 - \frac{m^2}{T^2}\right)^{3/2} \exp[-(n+1)y]
\end{aligned}$$

Now, define $t = (n+1)y$ and $x = (n+1)m/T$.

$$T \ln Z_{meson} = \frac{g_m V}{6\pi^2} T^4 \sum_{n=0}^\infty \frac{1}{(n+1)^4} \int_x^\infty dt \, \left(t^2 - x^2\right)^{3/2} \exp[-t]$$

Integer-order modified Bessel functions of the second kind are defined by

$$K_l(x) = \frac{2^l l!}{(2l)!} x^{-l} \int_x^\infty dt \, (t^2 - x^2)^{l-1/2} \exp(-t).$$

Using this in the above equation,

$$\begin{aligned} T \ln Z_{meson} &= \frac{g_m V}{6\pi^2} T^4 \sum_{n=0}^{\infty} \frac{1}{(n+1)^4} \frac{K_2(x)}{2^2 2! x^{-2}/(2.2)!} \\ &= \frac{g_m V}{2\pi^2} T^2 m^2 \sum_{n=0}^{\infty} \frac{1}{(n+1)^2} K_2\left(\frac{(n+1)m}{T}\right) \end{aligned}$$

Finally,

$$T \ln Z_{meson} = \frac{g_m V}{2\pi^2} T^2 m^2 \sum_{n=1}^{\infty} \frac{1}{n^2} K_2\left(\frac{nm}{T}\right)$$

We may now use Eq. (5.2) and Eq. (5.3) to compute the pressure and energy density for mesons. We use the relation $K_l'(x) = -K_{l-1}(x) - \frac{l}{x} K_l(x)$ for computing the derivative of $K_2(nm/T)$.

$$\boxed{P_{meson} = \frac{g_m}{2\pi^2} T^2 m^2 \sum_{n=1}^{\infty} \frac{1}{n^2} K_2\left(\frac{nm}{T}\right)}$$

$$\epsilon_{meson} = \frac{g_m}{2\pi^2} T^2 m^2 \left[3 \sum_{n=1}^{\infty} \frac{1}{n^2} K_2\left(\frac{nm}{T}\right) + \frac{m}{T} \sum_{n=1}^{\infty} \frac{1}{n} K_1\left(\frac{nm}{T}\right)\right]$$

$$\boxed{\epsilon_{meson} = 3P_{meson} + \frac{g_m}{2\pi^2} T m^3 \sum_{n=1}^{\infty} \frac{1}{n} K_1\left(\frac{nm}{T}\right)}$$

Now, we may turn to baryons, which are massive fermions.[18]

$$\begin{aligned} T \ln Z_{baryon} = \frac{g_b V}{6\pi^2} \int_0^{\infty} \frac{dk k^4}{\sqrt{k^2+m^2}} \Bigg[&\frac{1}{\exp\left[(\sqrt{k^2+m^2}-\mu)/T\right]+1} \\ &+ \frac{1}{\exp\left[(\sqrt{k^2+m^2}+\mu)/T\right]+1} \Bigg] \end{aligned} \tag{5.7}$$

$$\frac{1}{\exp[(\sqrt{k^2+m^2} \pm \mu)/T]+1} = \sum_{n=0}^{\infty} (-1)^n \exp\left[-\frac{(n+1)\sqrt{k^2+m^2}}{T}\right] exp\left[\mp \frac{(n+1)\mu}{T}\right]$$

Using the above relation in Eq. (5.7), the situation is almost identical to that in case of the mesonic partition function, since the extra exponential term and $(-1)^n$ in the above relation is just a multiplicative factor with no k dependence. Finally,

$$T \ln Z_{baryon} = \frac{g_b V}{2\pi^2} T^2 m^2 \sum_{n=1}^{\infty} \frac{(-1)^{n-1}}{n^2} K_2\left(\frac{nm}{T}\right) \left[\exp\left(\frac{n\mu}{T}\right) + \exp\left(-\frac{n\mu}{T}\right)\right]$$

We may agin use Eq. (5.2) and Eq. (5.3) to compute the pressure and energy density for baryons. Recall the relation $K_l'(x) = -K_{l-1}(x) - \frac{l}{x} K_l(x)$ for computing the derivative of $K_2(nm/T)$.

$$\boxed{P_{baryon} = \frac{g_b}{2\pi^2} T^2 m^2 \sum_{n=1}^{\infty} \frac{(-1)^{n-1}}{n^2} K_2\left(\frac{nm}{T}\right) \left[\exp\left(\frac{n\mu}{T}\right) + \exp\left(-\frac{n\mu}{T}\right)\right]}$$

$$\boxed{\epsilon_{baryon} = 3P_{baryon} + \frac{g_b}{2\pi^2} T m^3 \sum_{n=1}^{\infty} \frac{(-1)^{n-1}}{n} K_1\left(\frac{nm}{T}\right) \left[\exp\left(\frac{n\mu}{T}\right) + \exp\left(-\frac{n\mu}{T}\right)\right]}$$

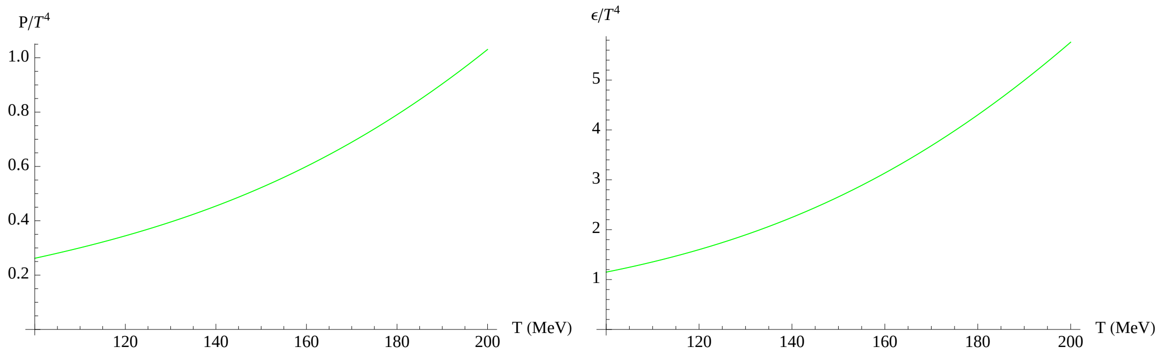

(a) Pressure of mesons as a function of temperature.

(b) Energy density of mesons as a function of temperature.

Figure 5.2: Total pressure and energy density of mesons listed in Appendix E.

Having obtained the partition functions for mesons and baryons, one still needs to sum over all the mesons and baryons with their respective masses and degrees of freedom to obtain the relationship between P and ϵ, and subsequently c_s^2, in the hadronic phase. The mass and degrees of freedom of mesons and baryons used[19] to perform the above calculation are tabulated in Appendix E. The pressure and

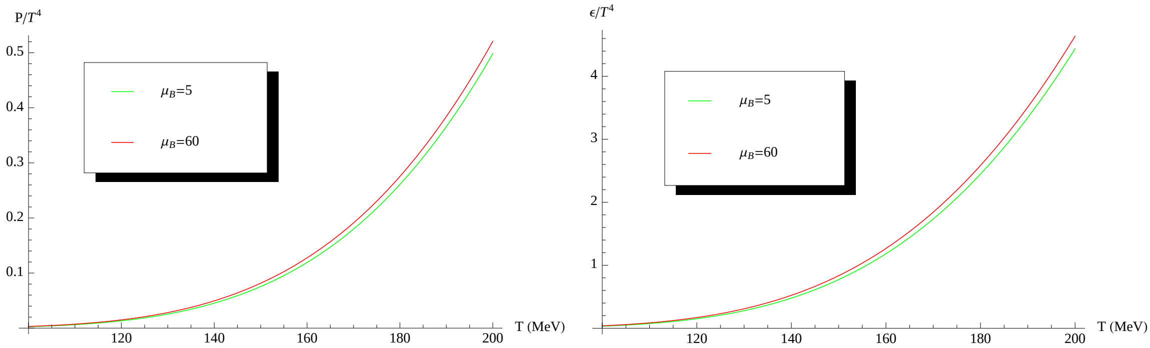

(a) Pressure of baryons as a function of temperature.

(b) Energy density of baryons as a function of temperature.

Figure 5.3: Total pressure and energy density of baryons listed in Appendix E.

energy density of mesons and baryons, as a function of temperature, are are plotted in Figure 5.2 and Figure 5.3 respectively.

5.2.3 Bag Pressure

At critical temperature, the pressure of the quark-gluon plasma and that of the hadronic gas is found to be unequal, as shown in Figure 5.4. This violates the criteria for mechanical equilibrium. Another term is needed to equalise the pressure and make

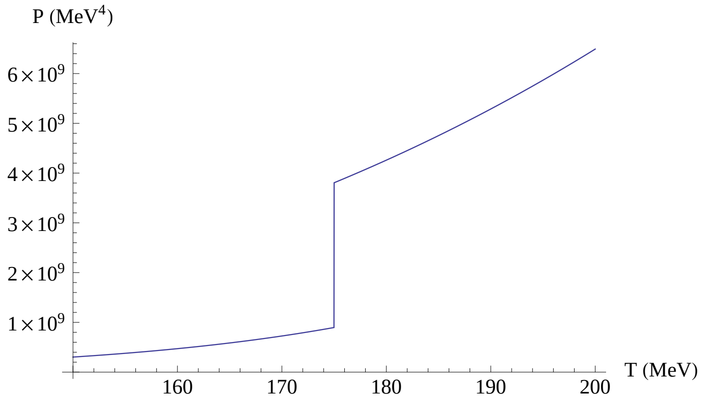

Figure 5.4: Pressure versus temperature, with QGP pressure (Section 5.2.1) above $T_c = 175$ MeV and hadronic pressure (Section 5.2.2) below T_c.

the transition possible. This additional pressure can be obtained by assuming that the quarks, whether confined to a single hadron or to the larger quark-gluon plasma, are contained within a field of constant positive potential energy per unit volume, referred to as B (for 'bag'). This potential energy was introduced in the model of hadron structure known as the *MIT bag model.*[20;21] The bag model includes both asymptotic freedom and confinement, the two main properties of QCD. Inside the bag, as long as the quark constituents of the hadron do not come too near the walls of the bag, they can be treated as free fields, the property of asymptotic freedom. However, when the quarks approach the bag surface, they are reflected back into the bag interior and so are confined to the bag interior, hence confinement.

In the bag model, the equations of motion are modified by the presence of the pressure relative to the free field but must still obey energy and momentum conservation.[18] The equations of motion are obtained from the energy-momentum tensor, $T^{\mu\nu}$. In the free field theory, $T^{\mu\nu} = T_0^{\mu\nu}$. The quarks in the bag are massless fermions and obey the Dirac equation,

$$i\partial\!\!\!/\psi(x) = 0.$$

The bag pressure introduces an additional term $-g^{\mu\nu}B$ along with the part given by massless fermions, giving us overall

$$T_{bag}^{\mu\nu} = (T_0^{\mu\nu} - g^{\mu\nu}B)\theta_V,$$

where the function θ_V is zero outside the bag but equal to unity inside.

Energy momentum conservation implies

$$\partial_\mu T_{bag}^{\mu\nu}(x) = 0.$$

$$\partial_\mu T_{bag}^{\mu\nu} = \partial(T_0^{\mu\nu} - g^{\mu\nu}B)\theta_V + (T_0^{\mu\nu} - g^{\mu\nu}B)\partial_\mu\theta_V = 0 \tag{5.8}$$

According to the definition of the canonical energy momentum tensor,[22] for the massless fermions, we can derive the energy momentum tensor using the definition of the massless Dirac Lagrangian

$$L_{Dirac} = \frac{i}{2}[\bar{\psi}\partial\!\!\!/\psi - \partial\!\!\!/\bar{\psi}\psi].$$

$$\begin{aligned} T_0^{\mu\nu} &= \frac{\partial L_{Dirac}}{\partial(\partial_\mu\psi)}\partial^\nu\psi + \frac{\partial L_{Dirac}}{\partial(\partial_\mu\bar{\psi})}\partial^\nu\bar{\psi} - g^{\mu\nu}L_{Dirac} \\ &= \frac{i}{2}\bar{\psi}\gamma^\mu\partial^\nu\psi - \frac{i}{2}(\partial^\nu\bar{\psi})\gamma^\mu\psi - g^{\mu\nu}L_{Dirac} \end{aligned} \tag{5.9}$$

The L_{Dirac} term is zero, since the field must obey the Dirac equation.

$$\partial_\mu T_0^{\mu\nu} = \frac{i}{2}\left[\partial\!\!\!/\bar{\psi}\partial^\nu\psi + \bar{\psi}\partial\!\!\!/\partial^\nu\psi - \partial\!\!\!/(\partial^\nu\bar{\psi})\psi - (\partial^\nu\bar{\psi})\partial\!\!\!/\psi\right]$$

Commuting the derivatives, the Dirac equation again renders all the terms to be zero. Note here that $\partial\!\!\!/\bar{\psi}$ is used to denote $\partial_\mu\bar{\psi}\gamma^\mu$. Hence, Eq. (5.8) becomes

$$(T_0^{\mu\nu} - g^{\mu\nu}B)\partial_\mu\theta_V = 0$$

From the definition of θ_V, it is easy to see that $\partial_\mu\theta_V = n_\mu\delta_V$, where δ_V is a delta function which is zero everywhere but on the surface and n_μ is the normal to the surface. Hence, to satisfy the above condition, we need

$$(T_0^{\mu\nu} - g^{\mu\nu}B)n_\mu\big|_{surface} = 0$$

Using Eq. (5.9), the above equation reduces to the boundary condition

$$\frac{i}{2}[\bar{\psi}n\!\!\!/\partial^\nu\psi - (\partial^\nu\bar{\psi})n\!\!\!/\psi] - n^\nu B = 0$$

The current $j^\mu = \bar{\psi}\gamma^\mu\psi\theta_V$ must also be conserved. Hence,

$$\begin{aligned} 0 = \partial_\mu j^\mu &= \partial\!\!\!/\bar{\psi}\psi\theta_V + \bar{\psi}\partial\!\!\!/\psi\theta_V + \bar{\psi}\gamma^\mu\psi\partial_\mu\theta_V \\ &= 0 + 0 + \bar{\psi}\gamma^\mu\psi n_\mu\delta_V \end{aligned}$$

Like before, this again implies that

$$\bar{\psi}\gamma^\mu\psi n_\mu\big|_{surface} = 0$$

As discussed above, quark-gluon plasma must satisfy asymptotic freedom and confinement, since we do not observe free quarks coming from the plasma in a heavy-ion collision. Thus the plasma can be thought of as being inside a larger version of the bag and we add a term to the free energy proportional to the bag pressure,

$$T \ln Z_{QGP(Bag)} = V \left[\pi^2 \left(\frac{g_g}{90} + \frac{7 g_q}{360} \right) T^4 + \frac{\mu_q^2 g_q}{12} T^2 + \frac{\mu_q^4 g_q}{24\pi^2} \right] - BV$$

Hence, using Eq. (5.2) and Eq. (5.3) again, we get

$$P_{QGP(Bag)} = \pi^2 \left(\frac{g_g}{90} + \frac{7 g_q}{360} \right) T^4 + \frac{\mu_q^2 g_q}{12} T^2 + \frac{\mu_q^4 g_q}{24\pi^2} - B$$

$$\epsilon_{QGP} = \pi^2 \left(\frac{g_g}{30} + \frac{7 g_q}{120} \right) T^4 + \frac{\mu_q^2 g_q}{4} T^2 + \frac{\mu_q^4 g_q}{8\pi^2} + B$$

With the additional term due to the bag pressure, it is possible to equalise the pressures at the critical temperature and make a first-order phase transition occur. For a fixed T_c, we can obtain the value of B.

5.2.4 Equation of State

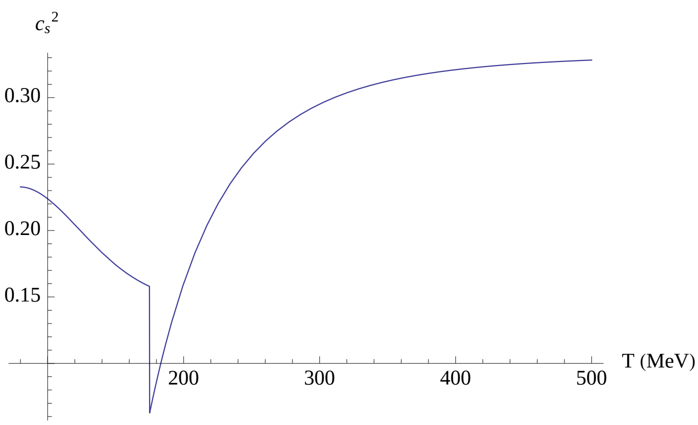

Figure 5.5: c_s^2 as a function of temperature as obtained from the bag model.

Once B is found by equalising the pressure at T_c for the QGP phase and the hadronic phase, one can obtain c_s^2 for the whole temperature range by computing the ratio of P to ϵ. The value of c_s^2, as a function of temperature, is given in Figure 5.5. The equations derived in Section 5.2.2 is used below the critical temperature and the equations derived in Section 5.2.3 are used above critical temperature. The critical temperature is assumed to be 175 MeV.

5.3 Lattice QCD

Lattice gauge theory is a way to probe the non-perturbative regime of QCD. QCD is asymptotically free at short distances where perturbative calculations are valid. When Feynman diagrams are evaluated, the large momenta corresponding to short distances may cause divergences in the momentum integrations, which are called "ultraviolet divergences". In perturbation theory, these are handled using renormalization group techniques. In non-perturbative QCD, the perturbative expansion is no longer valid and another strategy is required to handle the divergences.

Lattice gauge theory reformulates QCD on a lattice of discrete space-time points. The spacing between lattice points is finite. This lattice spacing gives a maximum momentum scale which acts as a momentum cut-off in the integrations, keeping them finite. Calculation are performed multiple times with different decreasing lattice distances a until the scaling regime is reached, where the lattice spacing is connected to a physical scale.

In lattice QCD, the partition function is computed using the path integral formulation. In Euclidean space, with imaginary time, the action is related to the Hamiltonian operator in the partition function and the imaginary time is related to the inverse temperature. The equation of state, that is the pressure as a function of energy density, can be obtained from lattice QCD calculations.[23] The value of c_s^2 as a function of temperature, as obtained from lattice calculations, is given in Figure 5.6.

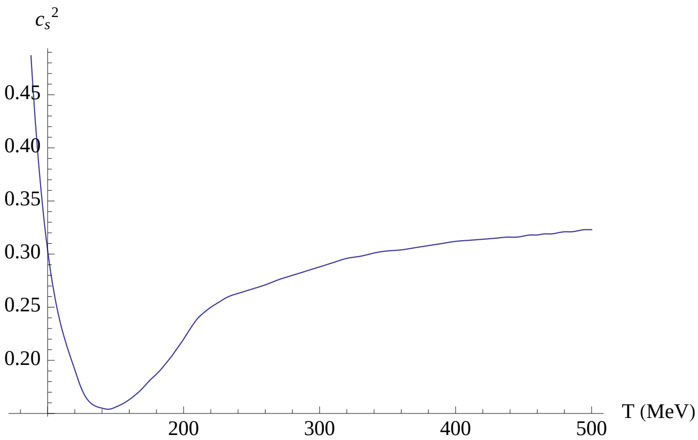

Figure 5.6: c_s^2 as a function of temperature as obtained from lattice calculations.[23]

Chapter 6

Hydrodynamics in 2+1 D

In Chapter 4, we solved the hydrodynamic equations by ignoring the transverse expansion of the system. Though the transverse expansion is small compared to the longitudinal expansion, while studying quantities like the transverse momentum spectrum, one cannot ignore its effect. If we do not ignore the velocity in the transverse direction, we get[24;18]

$$u^\mu = \frac{1}{\sqrt{1 - v_z^2 - v_r^2}}(1, v_z, v_r, 0). \tag{6.1}$$

It is sufficient to solve the hydrodynamic equations at $z = 0$, since we can then Lorentz boost it to find the solution at finite values of z.

6.1 Entropy Current Conservation Equation

Recall Eq. (3.5). Writing it out in vectorial form, we get

$$\frac{\partial(s\gamma)}{\partial t} + \nabla(s\gamma\vec{v}) = 0$$

If u^μ is of the particular form given in Eq. (6.1), this simplifies to

$$\frac{\partial(s\gamma)}{\partial t} + \frac{1}{r}\frac{\partial(rs\gamma v_r)}{\partial r} + \frac{\partial(s\gamma v_z)}{\partial z} = 0$$
$$\frac{\partial(s\gamma)}{\partial t} + \frac{1}{r}(s\gamma v_r) + \frac{\partial(s\gamma v_r)}{\partial r} + v_z\frac{\partial(s\gamma)}{\partial z} + \frac{1}{t}(s\gamma) = 0$$

As mentioned above, we will be looking at the solution at $z = 0$. Hence, we drop the terms linear in v_z.

$$\frac{\partial(s\gamma)}{\partial t} + \frac{\partial(s\gamma v_r)}{\partial r} + s\gamma\left(\frac{v_r}{r} + \frac{1}{t}\right) = 0 \tag{6.2}$$

6.2 Temperature Equation

Now, recall Eq. (3.8). We may use $u^\mu \partial_\mu = \gamma \frac{\partial}{\partial t} + \gamma \vec{v}.\nabla$ to write this out in vectorial form.

$$\gamma \frac{\partial(T(-\gamma\vec{v}))}{\partial t} + \gamma(\vec{v}.\nabla)(T(-\gamma\vec{v})) - \nabla T = 0$$

We may now use the vector identity $\vec{a}\times\vec{b}\times\vec{c} = \vec{b}(\vec{a}.\vec{c}) - \vec{c}(\vec{a}.\vec{b})$ to write $\vec{v}\times\nabla\times(T\gamma\vec{v}) = \nabla(T\gamma\vec{v}^2) - (\vec{v}.\nabla)(T\gamma\vec{v})$. Putting this in the above equation,

$$\gamma \frac{\partial(T\gamma\vec{v})}{\partial t} + \gamma\nabla(T\gamma\vec{v}^2) + \nabla T = \gamma\vec{v}\times\nabla\times(T\gamma\vec{v})$$

The right hand side will be zero since the fluid flow is irrotational. We may write $\gamma\nabla(T\gamma\vec{v}^2) = (\nabla T)\gamma^2\vec{v}^2 + \gamma T\nabla(\gamma\vec{v}^2)$ and use $\gamma^2\vec{v}^2 + 1 = \gamma^2$ to simplify the above expression to

$$\begin{aligned}
\gamma \frac{\partial(T\gamma\vec{v})}{\partial t} + \gamma T\nabla(\gamma\vec{v}^2) + \gamma^2\nabla T = 0 \\
\gamma \frac{\partial(T\gamma\vec{v})}{\partial t} + \gamma T\nabla(\gamma(\vec{v}^2 - 1)) + \gamma\nabla(\gamma T) = 0 \\
\frac{\partial(T\gamma\vec{v})}{\partial t} + \nabla(T\gamma) = 0
\end{aligned}$$

Again, if u^μ is of the particular form given in Eq. (6.1), at $z = 0$ this simplifies to

$$\frac{\partial(T\gamma v_r)}{\partial t} + \frac{\partial(T\gamma)}{\partial r} = 0 \tag{6.3}$$

6.3 Simplification

Since we are working where $v_z = 0$, one may define the boost angle $\alpha = \tanh^{-1} v_r$. This gives $v_r = \tanh\alpha$, $\gamma = \cosh\alpha$ and $\gamma v_r = \sinh\alpha$. Noting $\frac{\partial r}{\partial t} = 0$ and substituting these in Eq. (6.3) and Eq. (6.2) gives:

$$\begin{aligned}
\frac{\partial}{\partial t}(rts\cosh\alpha) + \frac{\partial}{\partial r}(rts\sinh\alpha) = 0 \\
\frac{\partial}{\partial t}(T\sinh\alpha) + \frac{\partial}{\partial r}(T\cosh\alpha) = 0
\end{aligned}$$

Expanding the derivatives, simplifying and substituting $v_r = \tanh\alpha$, we get:

$$\begin{aligned}\frac{\partial \ln s}{\partial t} + v_r\frac{\partial \ln s}{\partial r} + v_r\frac{\partial \alpha}{\partial t} + \frac{\partial \alpha}{\partial r} + \frac{1}{t} + \frac{v_r}{r} = 0\\ v_r\frac{\partial \ln T}{\partial t} + \frac{\partial \ln T}{\partial r} + \frac{\partial \alpha}{\partial t} + v_r\frac{\partial \alpha}{\partial r} = 0\end{aligned}$$

Recall $\frac{\partial \ln T}{\partial \ln s} = c_s^2$. Using this, we can define a ϕ such that $\partial\phi = c_s\partial\ln s = \frac{1}{c_s}\partial\ln T$. Using this, the above equations simplify to

$$\begin{aligned}\frac{\partial \phi}{\partial t} + v_r\frac{\partial \phi}{\partial r} + c_s v_r\frac{\partial \alpha}{\partial t} + c_s\frac{\partial \alpha}{\partial r} + c_s\left(\frac{1}{t} + \frac{v_r}{r}\right) = 0\\ v_r c_s\frac{\partial \phi}{\partial t} + c_s\frac{\partial \phi}{\partial r} + \frac{\partial \alpha}{\partial t} + v_r\frac{\partial \alpha}{\partial r} = 0\end{aligned}$$

We get two equations by adding the above two equations and subtracting the above two equations.

$$\begin{aligned}(1 + v_r c_s)\frac{\partial(\phi+\alpha)}{\partial t} + (v_r + c_s)\frac{\partial(\phi+\alpha)}{\partial r} + c_s\left(\frac{1}{t} + \frac{v_r}{r}\right) = 0\\ (1 - v_r c_s)\frac{\partial(\phi-\alpha)}{\partial t} + (v_r - c_s)\frac{\partial(\phi-\alpha)}{\partial r} + c_s\left(\frac{1}{t} + \frac{v_r}{r}\right) = 0\end{aligned}$$

Now, we can agin define $\ln a_\pm = \phi \pm \alpha$, which allows us to write the above equations in a compact form. Note that, in terms of the new variable, $\phi = \frac{1}{2}\ln a_+ a_-$ and $v_r = \frac{a_+ - a_-}{a_+ + a_-}$.

$$\frac{\partial a_\pm}{\partial t} + \frac{(v_r \pm c_s)}{(1 \pm v_r c_s)}\frac{\partial a_\pm}{\partial r} + \frac{c_s}{(1 \pm v_r c_s)}\left(\frac{1}{t} + \frac{v_r}{r}\right)a_\pm = 0$$

6.4 Characteristic Solution

We may use the method of characteristics to solve the above equation.[25] First, notice that

$$\frac{da_\pm(r,t)}{ds} = \frac{\partial a_\pm}{\partial t}\frac{dt}{ds} + \frac{\partial a_\pm}{\partial r}\frac{dr}{ds}.$$

Comparing this to the above equation, we get

$$\begin{aligned}
\frac{dt}{ds} &= 1 \\
\frac{dr}{ds} &= \frac{(v_r \pm c_s)}{(1 \pm v_r c_s)} \\
\frac{da_\pm}{ds} &= -\frac{c_s}{(1 \pm v_r c_s)} \left(\frac{1}{t} + \frac{v_r}{r} \right) a_\pm
\end{aligned}$$

What we have done above is essentially obtain the equation for a "charecteristic line" $s(r,t)$ along which $a_\pm$ is given by an ordinary differential equation.

The above equations can be solved numerically to obtain the hydrodynamic evolution of the system.

Chapter 7

Comparison to Experimental Output

As already discussed in Section 3.1, we only see hadrons for which hydrodynamics has already ceased to be applicable in experiments . Hence, it is of utmost importance to be able to generate predictions in terms of these hadrons from our calculations.

Fortunately, this can be done in a fairly straightforward fashion. The hydrodynamic equations itself do not know when to start or stop, so the first step is to supply these quantities. Since the colliding nuclei have to at least cross each other for the entire matter to behave like a fluid, we compute the time required for this from the speed and Lorentz contracted thickness of the nuclei and use this as the starting time. We may use a fixed energy density, at which the mean free path of the constituents is comparable to the system size, to stop the simulation. The yield of the hadrons can be calculated on this freeze out hypersurface by using the Cooper-Frey algorithm.[26]

The particles contained on the freeze out hypersurface can be still assumed to be in local thermal equilibrium, the hypersurface is the transition region from equilibrium to non-equilibrium. Under this assumption, the four current for a particular particle is given by

$$N^{\mu} = \int \frac{d^3\vec{p}}{E}\, p^{\mu} f.$$

where f is the distribution function for the particle, already discussed in Section 5.2. The number of particles dN crossing the freezeout surface element $d\sigma_{\mu}$ is $N^{\mu} d\sigma_{\mu}$.

Utilising the above definition, we can derive the invariant yield of the particle to be

$$\frac{d^3N}{d^3\vec{p}/E} = \int d\sigma^\mu \, p^\mu f.$$

In Chapter 4, we have already derived and simulated 1+1 D hydrodynamics using Bjorken initial condition. Standard codes are available for performing the same task and generating output which can be compared to experimental results.

7.1 BJ HYDRO

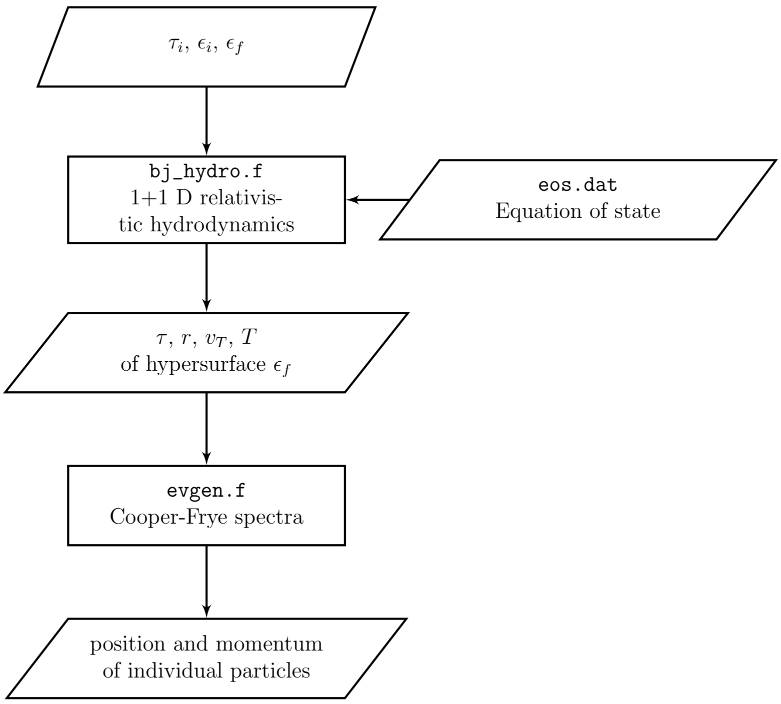

Figure 7.1: Flowchart summerising BJ HYDRO.

BJ HYDRO is an open source code which solves 1+1 D relativistic hydrodynamics with cylindrical symmetry and longitudinal Bjorken geometry.[27] Figure 7.1 summarises the general working of the code. Further details are given in the following sections.

7.1.1 Computation of the Hadronization Hypersurface (`bj_hydro.f`)

`bj_hydro.f` solves the fluid-dynamical equations of motion in 1+1 dimension and computes the hadronization hypersurface (or any other hypersurface of given energy density). Bjorken initial condition is assumed. Subsequently, one can generate the hadron phase-space distribution at hadronization using `evgen.f`.

Input

The following quantities may be specified:

- The initial time τ_i, in units of the transverse radius of the system.
- The initial energy density of the system, in units of critical pressure or $\epsilon_0 = 147.7$ MeV fm^{-3}.
- The equation of state to be used. One can use ideal gas, bag model or an arbitrary equation of state by specifying pressure as a function of energy density (both in units of $\epsilon_0 = 147.7$ MeV fm^{-3}) through the file `eos.dat`.
- The energy density of the hypersurface to be calculated, in units of critical pressure or $\epsilon_0 = 147.7$ MeV fm^{-3}.

Output

`hyper.dat` gives the hypersurface of the energy density specified. It gives the following quantities:

- (τ, r) in the plane $\phi = 0, \eta = 0$. Due to the assumed symmetry under rotations around the beam axis and Lorentz boosts along the beam axis, the hypersurface points (τ, r) are exactly the same at any other ϕ, η. The coordinates are reported in units of initial radius of the system.

- Transverse flow velocity
- Temperature

7.1.2 Generation of Particle Output from the Hypersurface (`evgen.f`)

The code `evgen.f` generates a table containing the momenta and space-time coordinates of each particle in the *Final Particle File Format - OSC1997A* output format. Longitudinal boost invariance, cylindrical and isospin symmetry etc. are assumed.

The hypersurface file `hyper.dat` is read. The space-time points on the hypersurface, the temperature, and the flow velocity at each point are used to calculate the continuous spectra of all hadron species, by employing the Cooper-Frye formula. The normalised hadron spectra are interpreted as probability distributions, from which individual events are generated randomly. The total number of hadrons of each species is the same in each event. Energy fluctuations are possible, since fluid dynamics determines only the average energy-momentum tensor. It is important to note that resonance decays are not performed in the code.

7.1.3 Results

The results produced using BJ HYDRO are given in Figure 7.2. At this point, we may recall the initial physical motivation described in Section 1.2. It is interesting to note that hydrodynamics has successfully reproduced the mass dependence of the invariant yield as a function of the transverse momentum. The rapidity distribution is also consistent with our assumption of Bjorken initial condition.

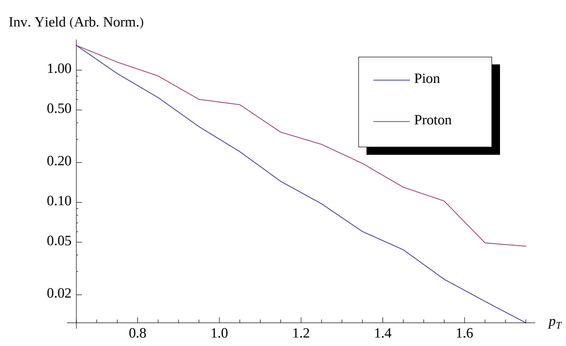

(a) p_T distribution generated using BJ HYDRO code.

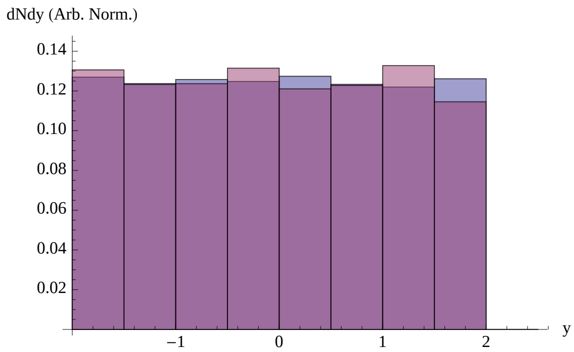

(b) y distribution generated using BJ HYDRO code.

Figure 7.2: Results generated by BJ HYDRO.

7.2 Outlook

The predictive power of hydrodynamic theory reaches far beyond just the particle spectrum. For a fundamental form of matter like QGP, transport coefficients, which is the proportionality constant between thermodynamic fluxes and the thermodynamic forces, is of great academic interest. If one includes viscosity, depending on how it is included, hydrodynamic theory is capable of making predictions regarding transport coefficients.

Table 7.1: Transport coefficients and their relationship with thermodynamic quantities

Flux	Force (∇ of)	Transport Coefficient	Equation
Momentum π_{ij}	Velocity v_i	Viscosity η	$\pi_{ij} = -\eta\left(\frac{\partial v_i}{\partial x_j}\right)$
Heat h_i	Temperature T	Heat Conductivity k	$h_i = -k\left(\frac{\partial T}{\partial x_i}\right)$
Diffusion flow Φ_i	Number density n	Diffusion constant D	$\Phi_i = -D\left(\frac{n}{\partial x_i}\right)$

Chapter 8

Conclusion

This master's thesis is based on a simple observation in relativistic heavy-ion collisions, that the slope of the momentum distribution of the produced hadrons in the collisions shows a mass dependence. Specifically, it is observed that the slope increases with mass of the hadron species under consideration. Since the slope of the momentum distribution of a dynamic thermal system is a joint measure of the temperature and collectivity, the mass dependence of the slope is attributed to hydrodynamics-like behaviour of the relativistic fluid formed in high energy heavy-ion collisions. However, subsequent observation of mass dependence of the slope of momentum distribution in proton-nucleus collisions puts forth the following question: Is the physical mechanism behind the mass dependence of slope of momentum distribution of hadrons the same for nucleus-nucleus collisions, where you expect the system to be big enough for applying hydrodynamics, and nucleon-nucleus collisions, where the very applicability of hydrodynamics is questionable?

In the first part of the thesis, we investigated two phenomenological approaches—one based on random walk, called the random walk model, and another inspired by hydrodynamics, called the blast wave model. We demonstrated that the random walk model explains the mass dependence of the nucleon-nucleus momentum distribution well, but fails completely for the nucleus-nucleus system. On the other hand the blast-wave model, which models the mass dependence of collectivity (as in hydrodynamics), explains the nucleus-nucleus results well. Thus, we established that possibly the dominant underlying physical mechanism for mass dependence of the slope of transverse momentum distribution of hadrons in nucleon-nucleus and nucleus-nucleus collisions are different. While that for nucleon-nucleus collisions could be due to random walk-like effects in the system, that for nucleus-nucleus collisions is probably due to the collectivity developed in the system.

Having established the importance of hydrodynamics in relativistic systems like nucleus-nucleus collisions, in the subsequent part of the thesis, we turned our attention to hydrodynamic modelling of the system. This involved setting up the hydrodynamic equations (without viscosity) in 1+1 dimensions and 2+1 dimensions. The 1+1 dimensional equations were solved. Initial conditions proposed by J. D. Bjorken were used. There existed three equations with four variables, which demanded another equation to be supplied externally. The equation of state of the system, which is just the functional relation between pressure and energy density or the speed of sound in the medium, was used. We solved the 1+1 dimensional hydrodynamic equations with three different equations of state—that of an ideal gas of quarks, gluons and hadrons, that prescribed by MIT Bas Model (detailed discussion of the approach formed a major part of this thesis) and finally, the equation of state that comes from first principle calculation of QCD using lattice gauge theory. We contrasted the evolution of initial energy density of the system for the three different equations of state and realised that the fastest cooling rate is for the ideal equation of state. Finally, the space-time coordinates of the freeout hypersurface of the fluid, the temperature and the flow velocity was used to calculate the continuous momentum spectra of the hadrons. Technically this approach of converting fluid elements as in hydrodynamic modelling to particles is called the Cooper-Frey approach. We observed that the particle spectra obtained solving the hydrodynamic equations faithfully produced the mass dependence of the slope of momentum distribution of produced hadrons, thereby providing a sound theoretical basis for our earlier claim that collectivity is the physical phenomena responsible for the of mass dependence of slope of momentum distribution of produced hadrons in high energy heavy-ion collisions. The system of high energy heavy-ion collisions provided a unique opportunity to apply thermodynamics, hydrodynamics, relativity, quantum mechanics, particle physics and quantum chromodynamics in a single system.

References

[1] László P Csernai. *Introduction to relativistic heavy ion collisions*. Wiley New York, 1994.

[2] Tapan K. Nayak. Heavy Ions: Results from the Large Hadron Collider. *Pramana*, 79:719–735, 2012. doi: 10.1007/s12043-012-0373-7.

[3] A. Leonidov, M. Nardi, and H. Satz. Hadron spectra from nuclear collisions. *Z.Phys.*, C74:535–540, 1997. doi: 10.1007/s002880050416.

[4] Jan-e Alam, J. Cleymans, K. Redlich, and H. Satz. What can we learn from transverse momentum spectra in relativistic heavy ion collisions? 1997.

[5] Ekkard Schnedermann, Josef Sollfrank, and Ulrich Heinz. Thermal phenomenology of hadrons from 200 *A* gev s+s collisions. *Phys. Rev. C*, 48:2462–2475, Nov 1993. doi: 10.1103/PhysRevC.48.2462. URL `http://link.aps.org/doi/10.1103/PhysRevC.48.2462`.

[6] Kirill Tuchin. Particle production in strong electromagnetic fields in relativistic heavy-ion collisions. *Adv.High Energy Phys.*, 2013:490495, 2013. doi: 10.1155/2013/490495.

[7] Ulrich Heinz, Ekkard Schnedermann, and Kang S. Lee. *HADRONIZATION OF A QUARK-GLUON PLASMA*, chapter 9, pages 471–517. doi: 10.1142/9789814503297_0009. URL `http://www.worldscientific.com/doi/abs/10.1142/9789814503297_0009`.

[8] J. D. Bjorken. Highly relativistic nucleus-nucleus collisions: The central rapidity

region. *Phys. Rev. D*, 27:140–151, Jan 1983. doi: 10.1103/PhysRevD.27.140. URL `http://link.aps.org/doi/10.1103/PhysRevD.27.140`.

[9] Michael L. Miller, Klaus Reygers, Stephen J. Sanders, and Peter Steinberg. Glauber modeling in high-energy nuclear collisions. *Annual Review of Nuclear and Particle Science*, 57(1):205–243, 2007. doi: 10.1146/annurev.nucl.57.090506.123020.

[10] P.V. Ruuskanen. Transverse Hydrodynamics With a First Order Phase Transition in Very High-energy Nuclear Collisions. *Acta Phys.Polon.*, B18:551, 1987.

[11] Steven N. Shore. *An Introduction to Astrophysical Hydrodynamics*. Academic Press, 1992. ISBN 0126406707.

[12] Sanjay P Sane. The aerodynamics of insect flight. *The journal of experimental biology*, 206(23):4191–4208, 2003.

[13] Edmond Iancu. Theory summary for ISMD2000. pages 411–437, 2011. doi: 10.5689/UA-PROC-2010-09/58.

[14] S.Z. Belenkji and L.D. Landau. Hydrodynamic theory of multiple production of particles. *Il Nuovo Cimento*, 3(1):15–31, 1956. ISSN 0029-6341. doi: 10.1007/BF02745507. URL `http://dx.doi.org/10.1007/BF02745507`.

[15] Herbert Goldstein. *Classical mechanics*. Addison Wesley, San Francisco, 2002. ISBN 0201657023.

[16] Kerson Huang. *Statistical Mechanics, 2nd Edition*. Wiley, 1987. ISBN 0471815187.

[17] Pathria Beale. *Statistical Mechanics*. 2011. ISBN 9380931891.

[18] Ramona Vogt. *Ultrarelativistic Heavy-Ion Collisions.* Elsevier Science, 2007. ISBN 0444521968.

[19] Particle Data Group. *Particle Physics Booklet.* Institute of Physics publishing, 2012.

[20] A. Chodos, R. L. Jaffe, K. Johnson, C. B. Thorn, and V. F. Weisskopf. New extended model of hadrons. *Phys. Rev. D*, 9: 3471–3495, Jun 1974. doi: 10.1103/PhysRevD.9.3471. URL `http://link.aps.org/doi/10.1103/PhysRevD.9.3471`.

[21] T. DeGrand, R. L. Jaffe, K. Johnson, and J. Kiskis. Masses and other parameters of the light hadrons. *Phys. Rev. D*, 12:2060–2076, Oct 1975. doi: 10.1103/PhysRevD.12.2060. URL `http://link.aps.org/doi/10.1103/PhysRevD.12.2060`.

[22] Walter Greiner and Joachim Reinhardt. *Field Quantization.* Springer, 1996. ISBN 3540591796.

[23] Szabolcs Borsnyi, Zoltn Fodor, Christian Hoelbling, Sndor D. Katz, Stefan Krieg, and Klmn K. Szab. Full result for the {QCD} equation of state with flavors. *Physics Letters B*, 730(0):99 – 104, 2014. ISSN 0370-2693. doi: http://dx.doi.org/10.1016/j.physletb.2014.01.007. URL `http://www.sciencedirect.com/science/article/pii/S0370269314000197`.

[24] Gordon Baym, Bengt L Friman, J-P Blaizot, M Soyeur, and W Czyż. Hydrodynamics of ultra-relativistic heavy ion collisions. *Nuclear physics A*, 407(3): 541–570, 1983.

[25] F. John. *Partial Differential Equations.* Number v. 1 in Applied

Mathematical Sciences. Springer, 1982. ISBN 9780387906096. URL `http://books.google.co.in/books?id=cBib_bsGGLYC`.

[26] Fred Cooper, Graham Frye, and Edmond Schonberg. Landau's hydrodynamic model of particle production and electron-positron annihilation into hadrons. *Phys. Rev. D*, 11:192–213, Jan 1975. doi: 10.1103/PhysRevD.11.192. URL `http://link.aps.org/doi/10.1103/PhysRevD.11.192`.

[27] Adrian Dumitru and Dirk H. Rischke. BJ HYDRO. `https://karman.physics.purdue.edu/OSCAR/index.php/BJ_HYDRO`, 2000.

[28] B. Alper et al. The Production of Charged Particles with High Transverse Momentum in Proton Proton Collisions at the CERN ISR. *Nucl.Phys.*, B87:19, 1975. doi: 10.1016/0550-3213(75)90248-5.

[29] B. Alper et al. Production Spectra of pi+-, K+-, rho+- at Large Angles in Proton Proton Collisions in the CERN Intersecting Storage Rings. *Nucl.Phys.*, B100:237, 1975. doi: 10.1016/0550-3213(75)90618-5.

[30] John Adams et al. phi meson production in Au + Au and p+p collisions at s(NN)**(1/2) = 200-GeV. *Phys.Lett.*, B612:181–189, 2005. doi: 10.1016/j.physletb.2004.12.082.

[31] T. Abbott et al. Measurement of particle production in proton induced reactions at 14.6-GeV/c. *Phys.Rev.*, D45:3906–3920, 1992. doi: 10.1103/PhysRevD.45.3906.

[32] H. Boggild et al. Charged kaon and pion production at mid-rapidity in proton nucleus and sulphur nucleus collisions. *Phys.Rev.*, C59:328–335, 1999. doi: 10.1103/PhysRevC.59.328.

[33] Betty Bezverkhny Abelev et al. Multiplicity Dependence of Pion, Kaon, Proton and Lambda Production in p–Pb Collisions at $\sqrt(s_N N) = 5.02$ TeV. 2013.

[34] Serguei Chatrchyan et al. Study of the production of charged pions, kaons, and protons in pPb collisions at $\sqrt{s_{NN}} = 5.02$ TeV. 2013.

[35] S.V. Afanasiev et al. Energy dependence of pion and kaon production in central Pb + Pb collisions. *Phys.Rev.*, C66:054902, 2002. doi: 10.1103/PhysRevC.66.054902.

[36] B.I. Abelev et al. Systematic Measurements of Identified Particle Spectra in pp, d^+ Au and Au+Au Collisions from STAR. *Phys.Rev.*, C79:034909, 2009. doi: 10.1103/PhysRevC.79.034909.

[37] T. Anticic et al. Centrality dependence of proton and antiproton spectra in Pb+Pb collisions at 40A GeV and 158A GeV measured at the CERN SPS. *Phys.Rev.*, C83:014901, 2011. doi: 10.1103/PhysRevC.83.014901.

[38] Betty Abelev et al. Centrality dependence of π, K, p production in Pb-Pb collisions at $\sqrt{s_{NN}} = 2.76$ TeV. *Phys.Rev.*, C88:044910, 2013. doi: 10.1103/PhysRevC.88.044910.

Table 8.1: Source of collision data used in analysis

Event	Reference
pp	Alper et al.[28], Alper et al.[29], Adams et al.[30]
pA	Abbott et al.[31], Boggild et al.[32], Abelev et al.[33], Chatrchyan et al.[34]
dAu	Adams et al.[30]
AA	Afanasiev et al.[35], Abelev et al.[36], Anticic et al.[37], Abelev et al.[38]

Appendix A

Fits of $p - p$ collisions using random walk model

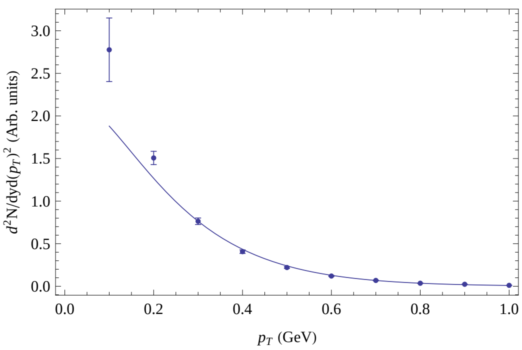

(a) 23 GeV

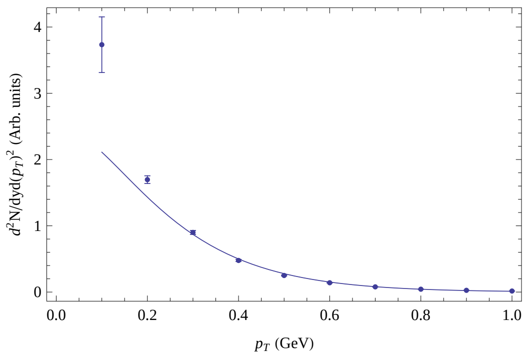

(b) 31 GeV

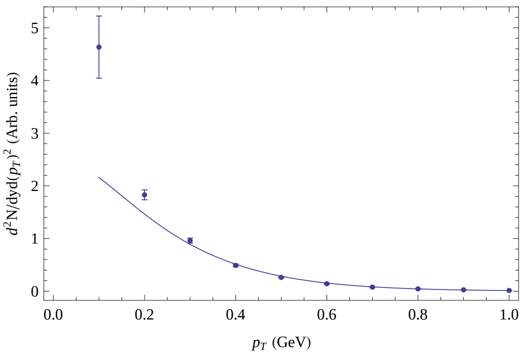

(c) 45 GeV

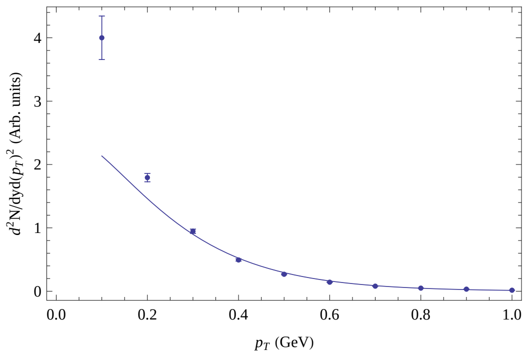

(d) 53 GeV

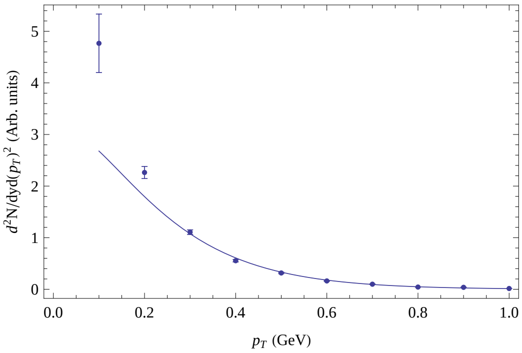

(e) 63 GeV

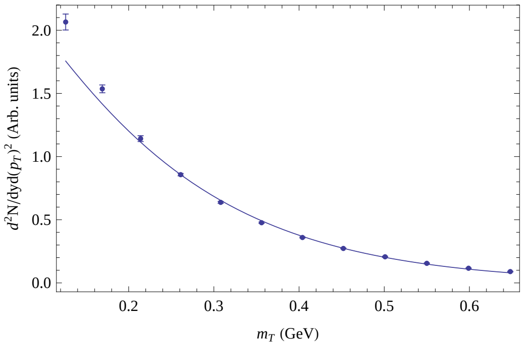

(f) 200 GeV

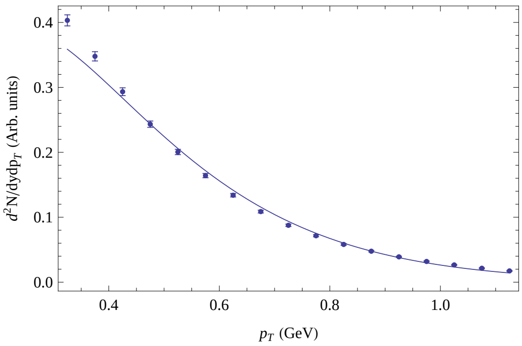

(g) 900 GeV

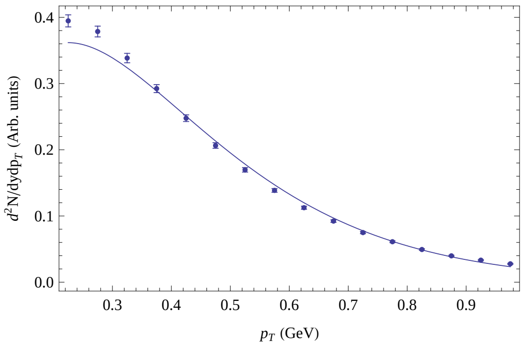

(h) 2760 GeV

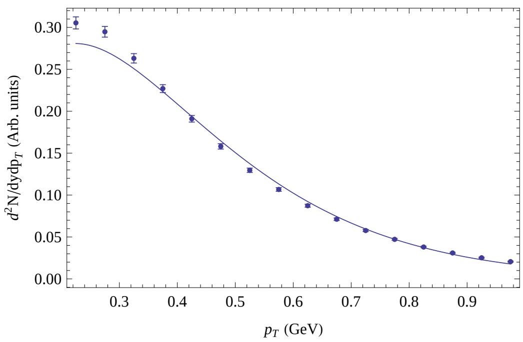

(i) 7000 GeV

Figure A.1: Fits for π^+ yield in $p - p$ collisions.

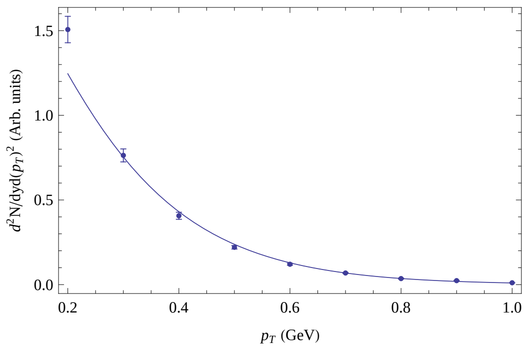

(a) 23 GeV

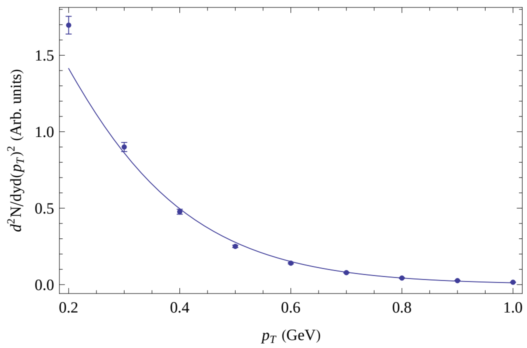

(b) 31 GeV

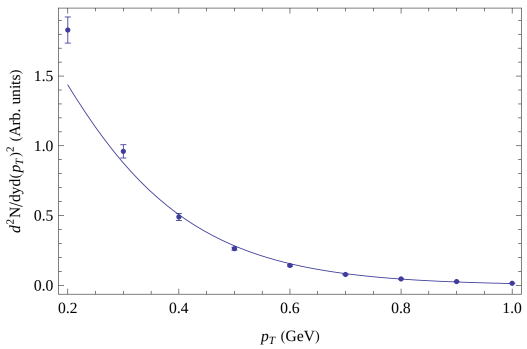

(c) 45 GeV

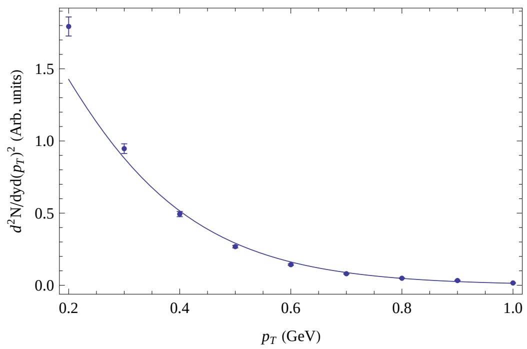

(d) 53 GeV

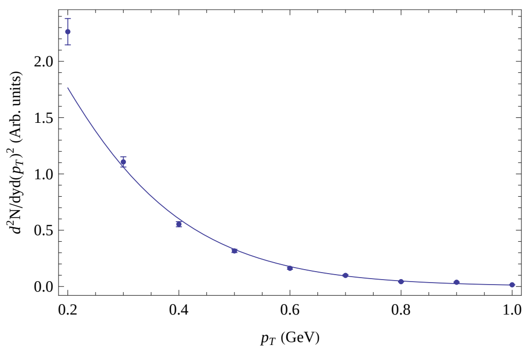

(e) 63 GeV

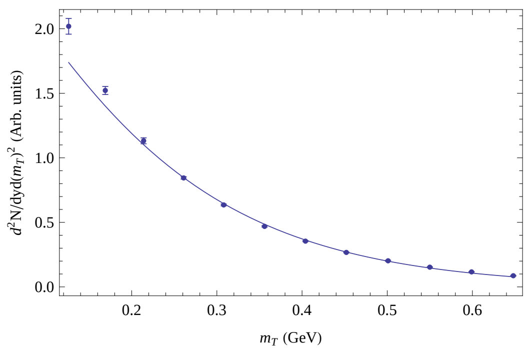

(f) 200 GeV

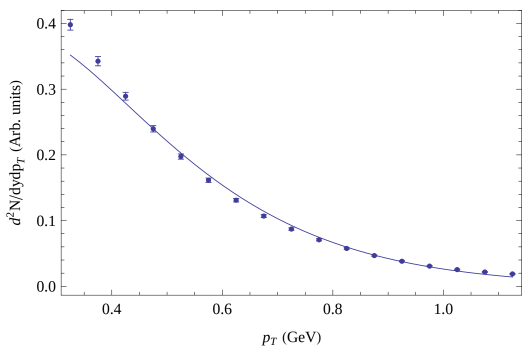

(g) 900 GeV

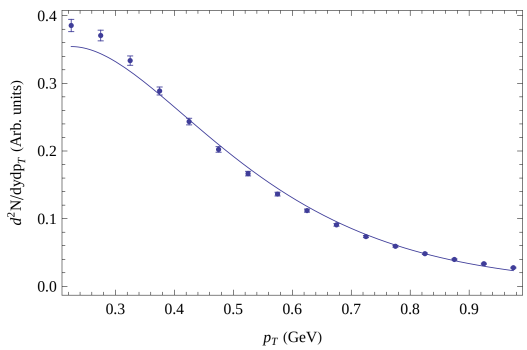

(h) 2760 GeV

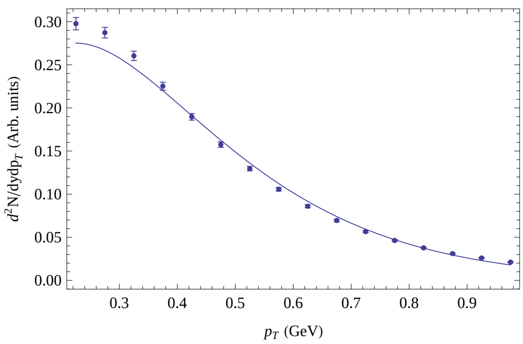

(i) 7000 GeV

Figure A.2: Fits for π^- yield in $p - p$ collisions.

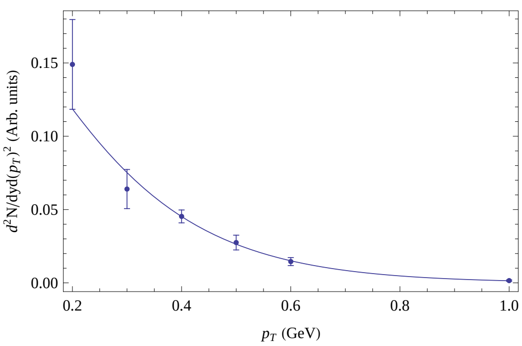

(a) 23 GeV

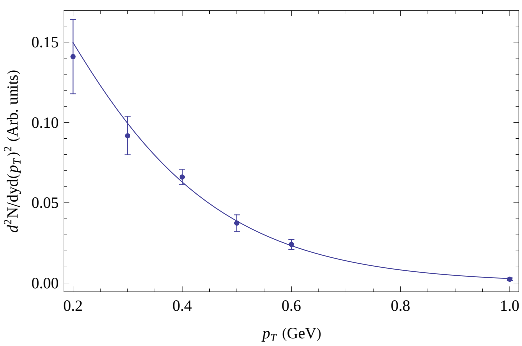

(b) 31 GeV

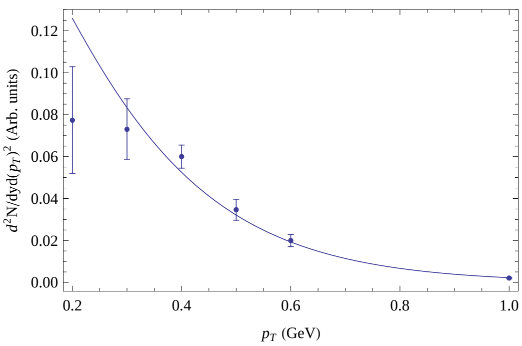

(c) 45 GeV

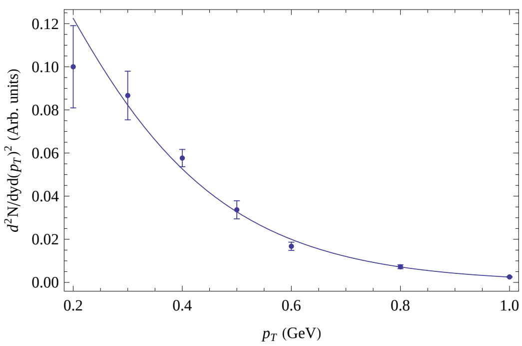

(d) 53 GeV

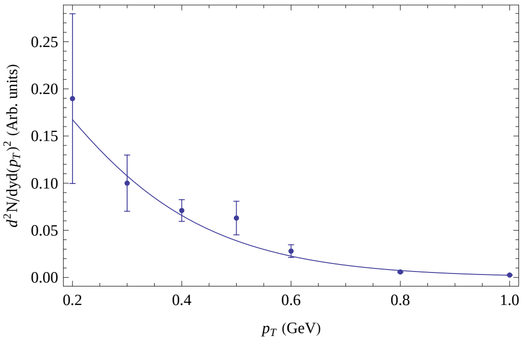

(e) 63 GeV

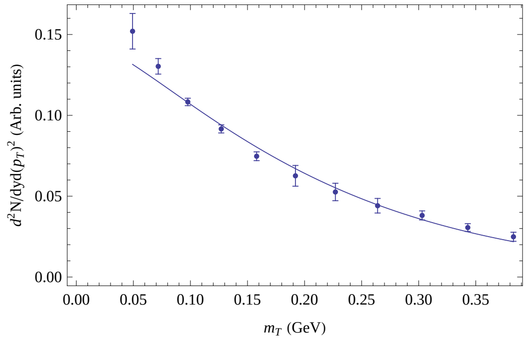

(f) 200 GeV

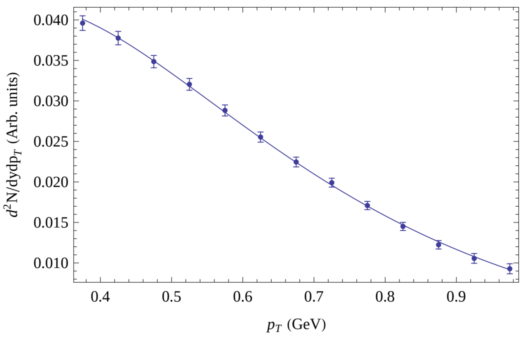

(g) 900 GeV

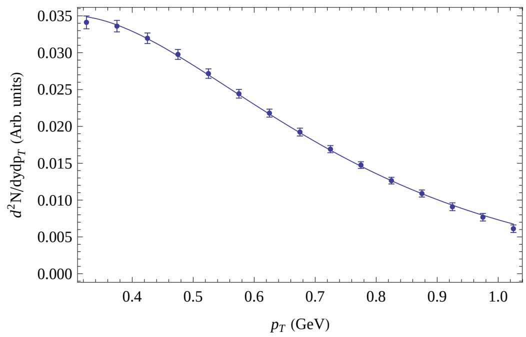

(h) 2760 GeV

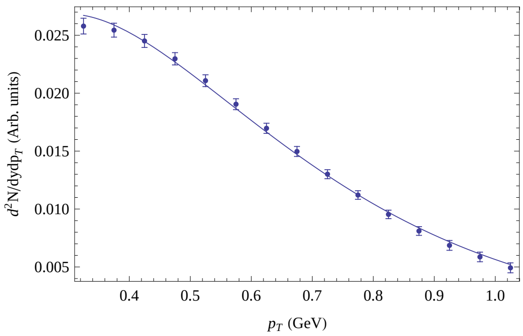

(i) 7000 GeV

Figure A.3: Fits for K^+ yield in $p-p$ collisions.

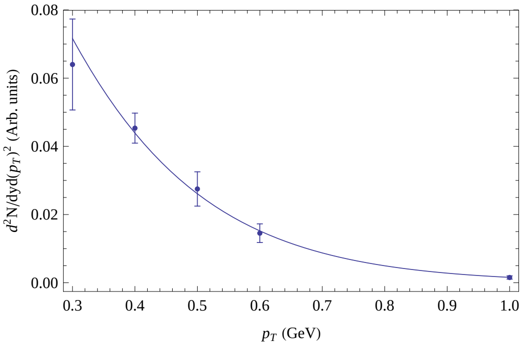

(a) 23 GeV

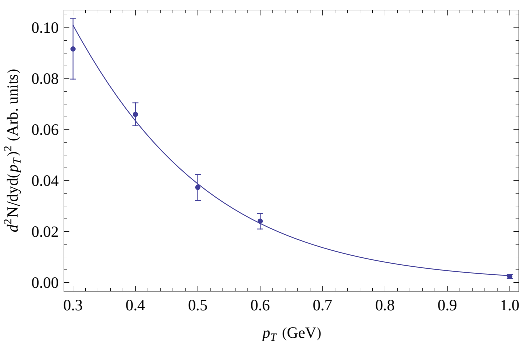

(b) 31 GeV

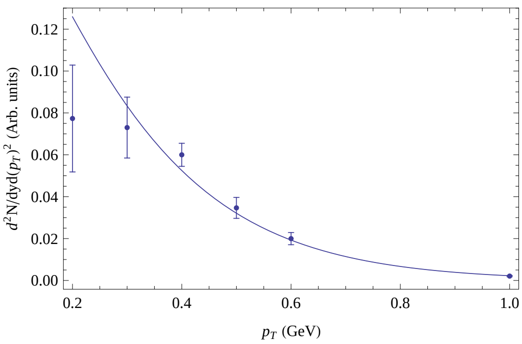

(c) 45 GeV

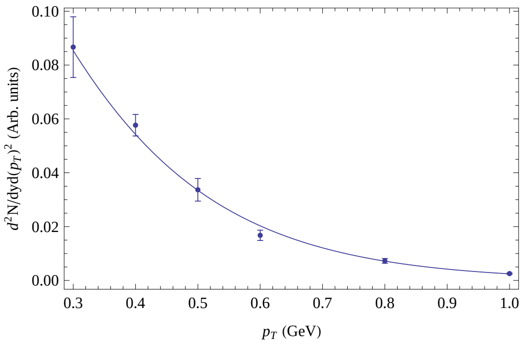

(d) 53 GeV

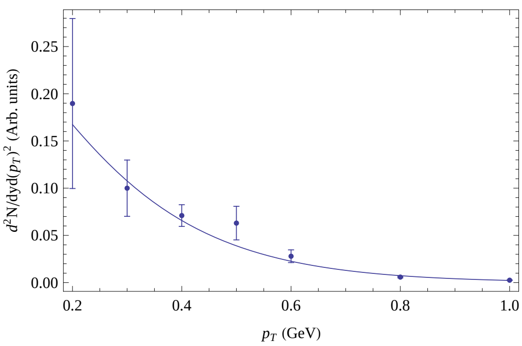

(e) 63 GeV

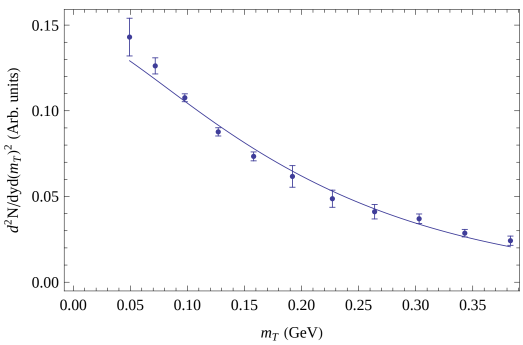

(f) 200 GeV

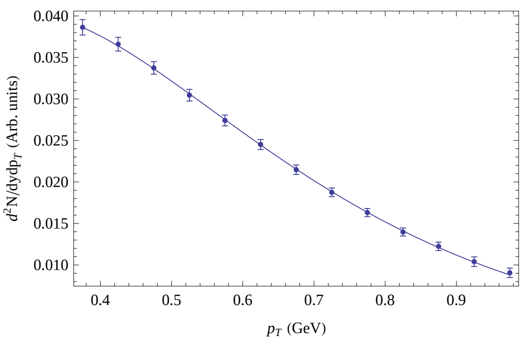

(g) 900 GeV

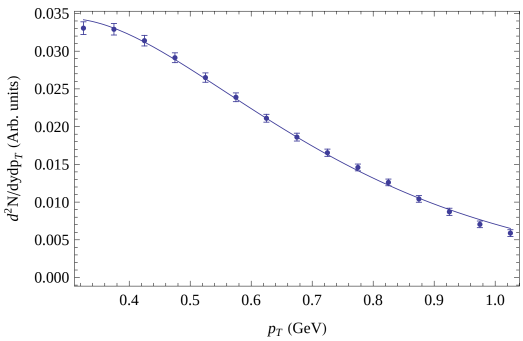

(h) 2760 GeV

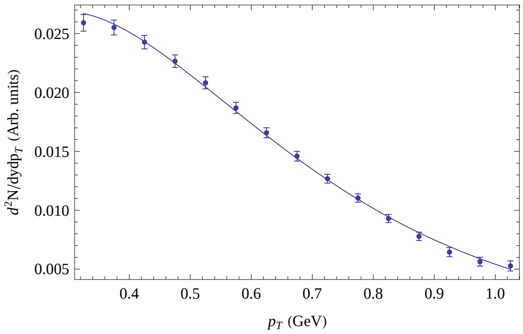

(i) 7000 GeV

Figure A.4: Fits for K^- yield in $p-p$ collisions.

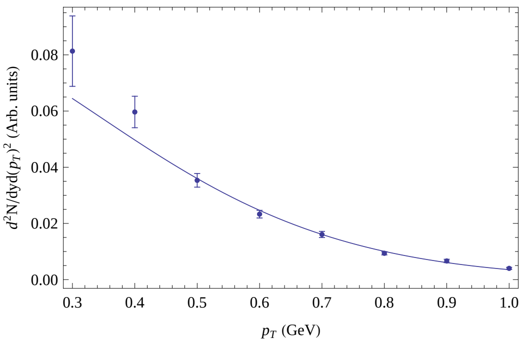

(a) 23 GeV

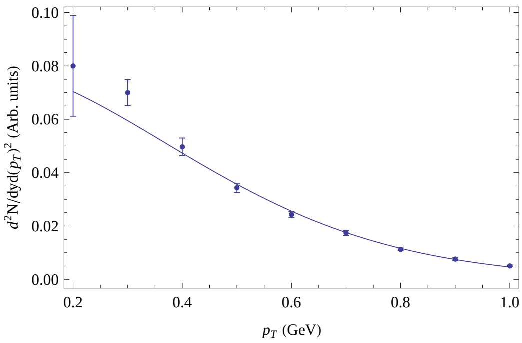

(b) 31 GeV

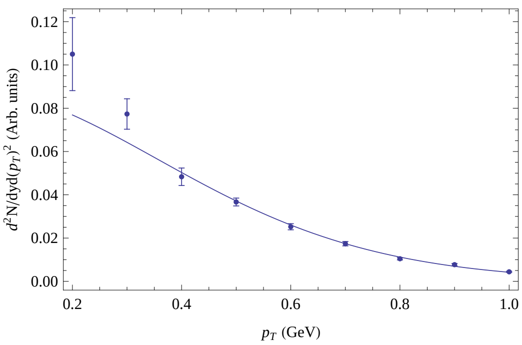

(c) 45 GeV

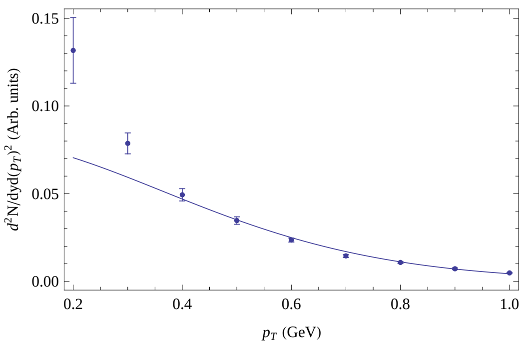

(d) 53 GeV

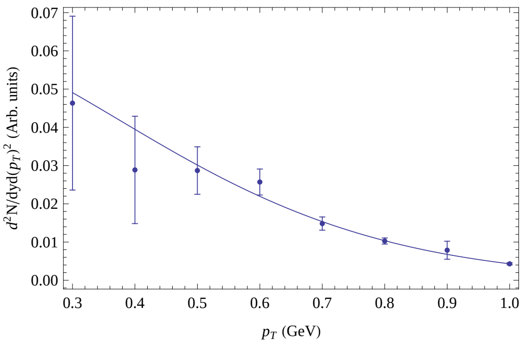

(e) 63 GeV

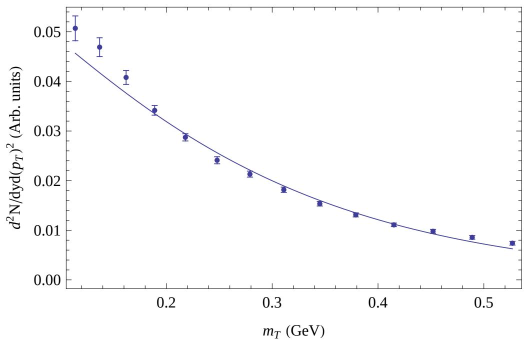

(f) 200 GeV

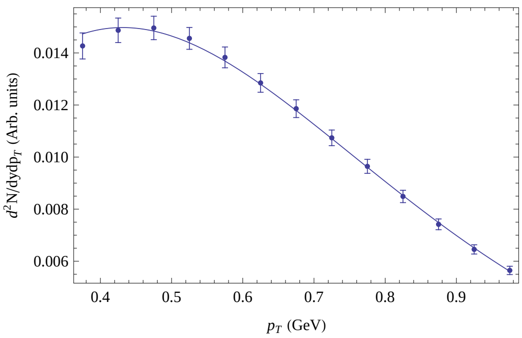

(g) 900 GeV

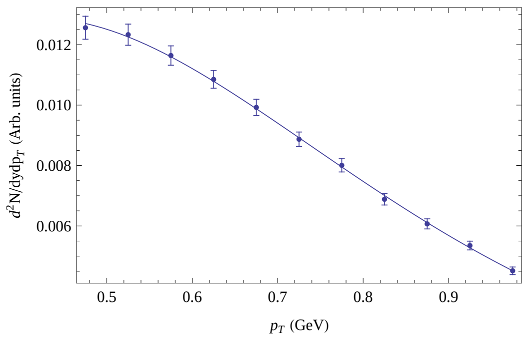

(h) 2760 GeV

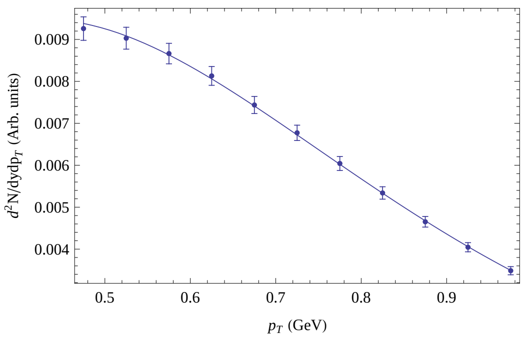

(i) 7000 GeV

Figure A.5: Fits for p yield in $p-p$ collisions.

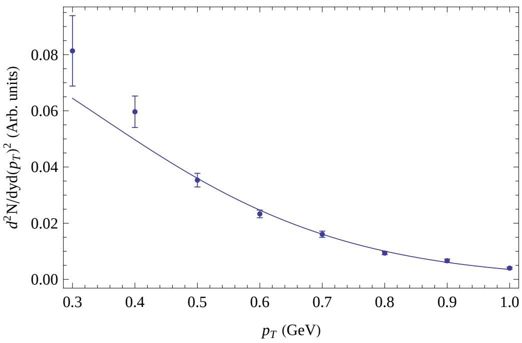

(a) 23 GeV

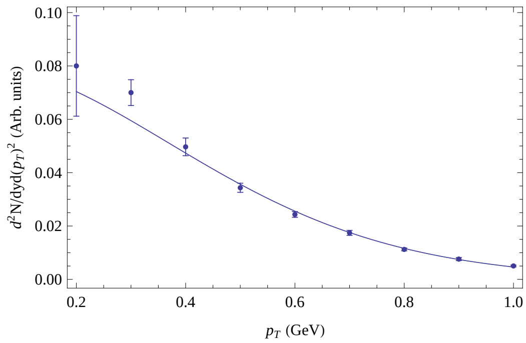

(b) 31 GeV

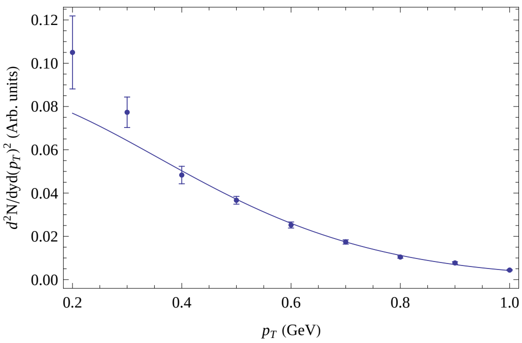

(c) 45 GeV

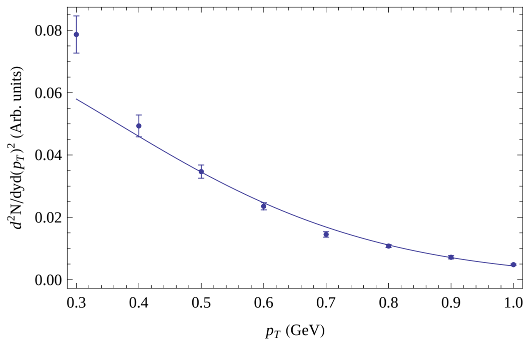

(d) 53 GeV

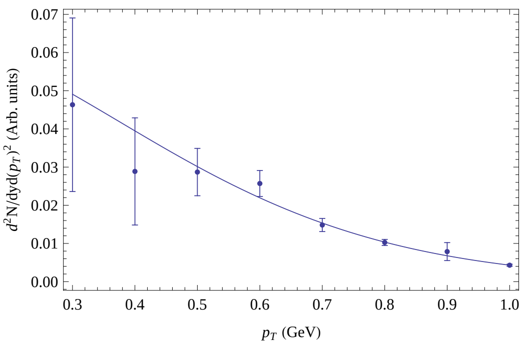

(e) 63 GeV

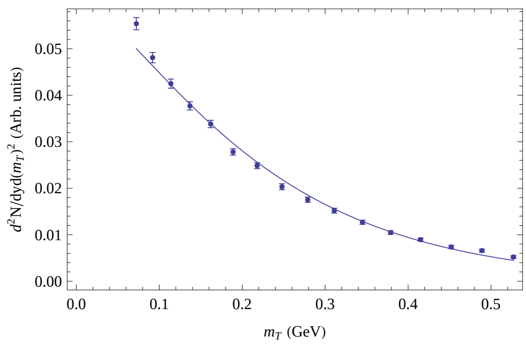

(f) 200 GeV

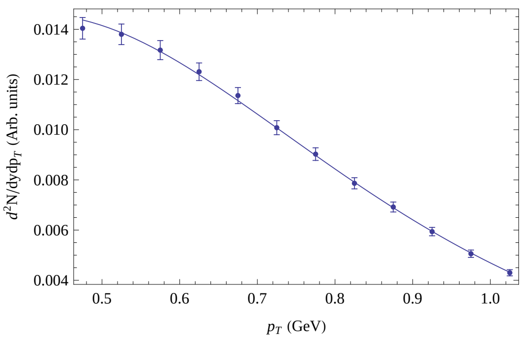

(g) 900 GeV

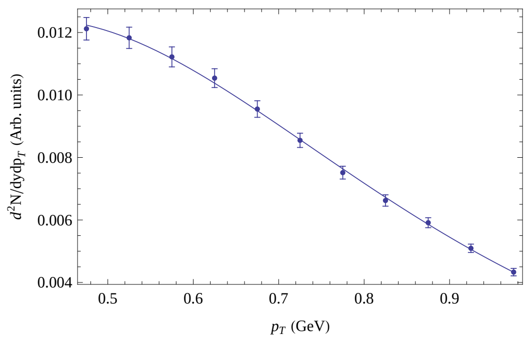

(h) 2760 GeV

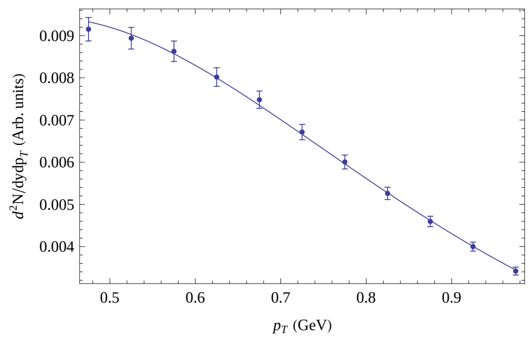

(i) 7000 GeV

Figure A.6: Fits for $\bar{p}$ yield in $p-p$ collisions.

Appendix B

Fits of $p - A$ collisions using random walk model

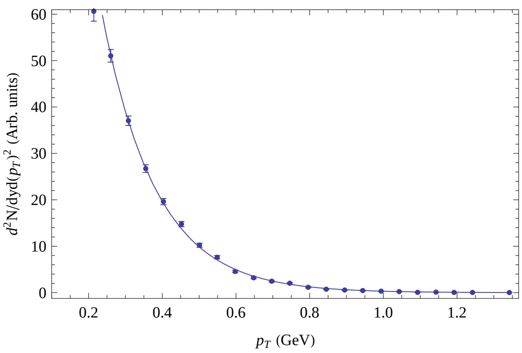

(a) π^+ in $p - Be$ at 5.4 GeV

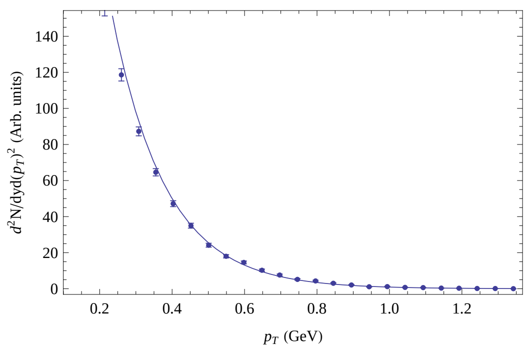

(b) π^+ in $p - Al$ at 5.4 GeV

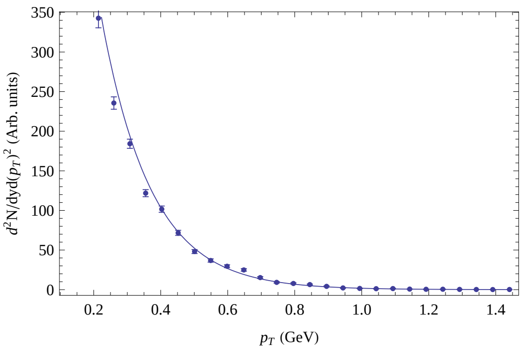

(c) π^+ in $p - Cu$ at 5.4 GeV

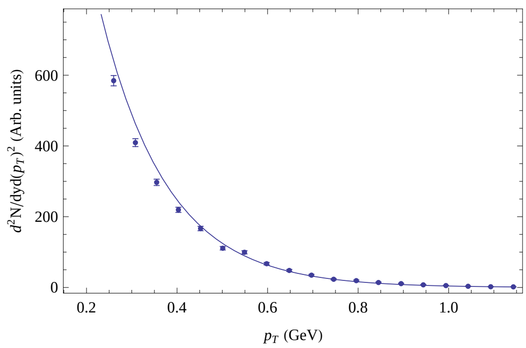

(d) π^+ in $p - Au$ at 5.4 GeV

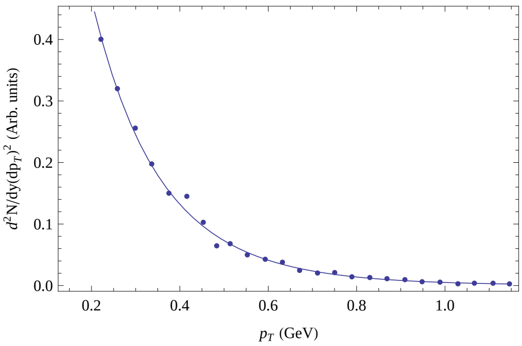

(e) π^+ in $p-Pb$ at 450 AGeV

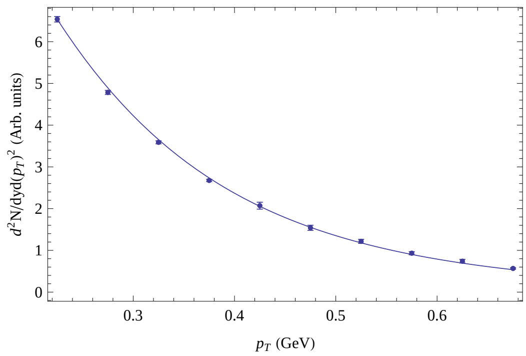

(f) π^+ in $d-Au$ at 200 GeV

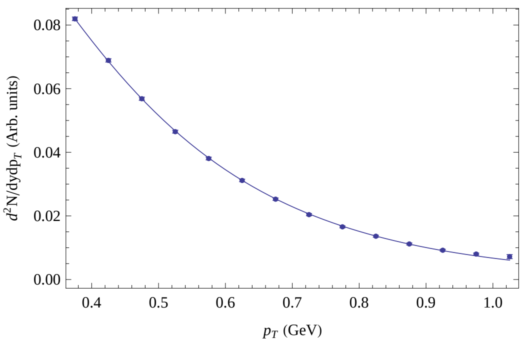

(g) π^+ in $p-Pb$ at 5020 GeV

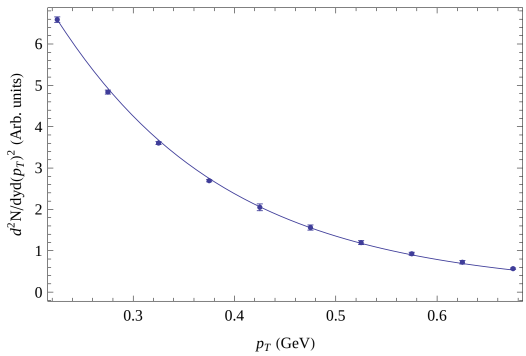

(h) π^- in $d-Au$ at 200 GeV

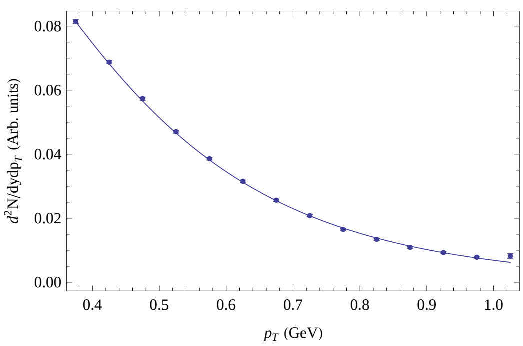

(i) π^- in $p-Pb$ at 5020 GeV

Figure B.1: Fits for π^+ and π^- yield in $p-A$ collisions.

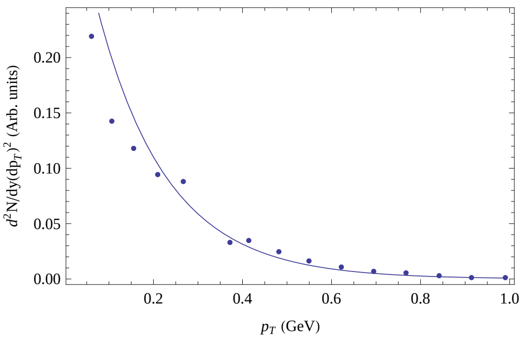

(a) K^+ in $p - Pb$ at 450 AGeV

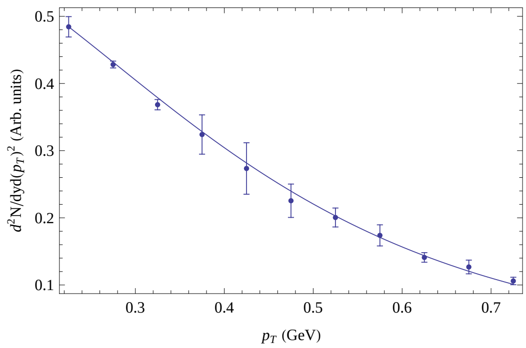

(b) K^+ in $d - Au$ at 200 GeV

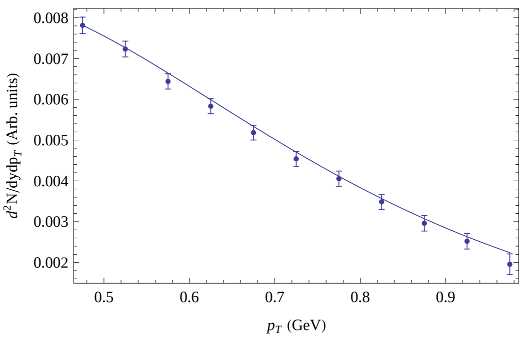

(c) K^+ in $p - Pb$ at 5020 GeV

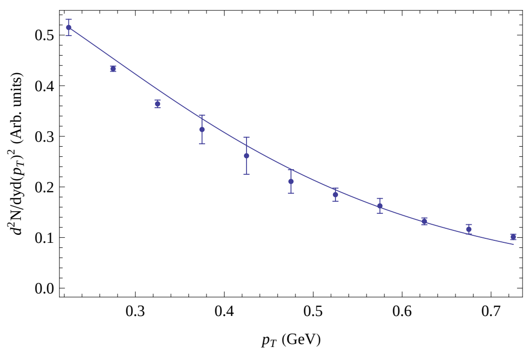

(d) K^- in $d - Au$ at 200 GeV

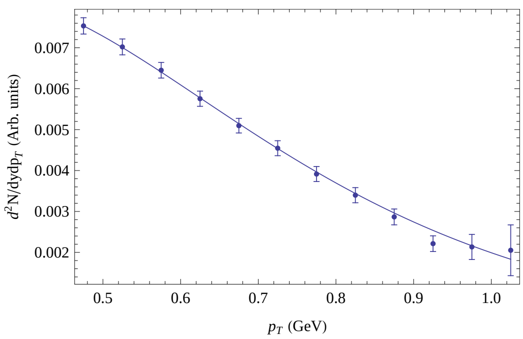

(e) K^- in $p - Pb$ at 5020 GeV

Figure B.2: Fits for K^+ and K^- yield in $p - A$ collisions.

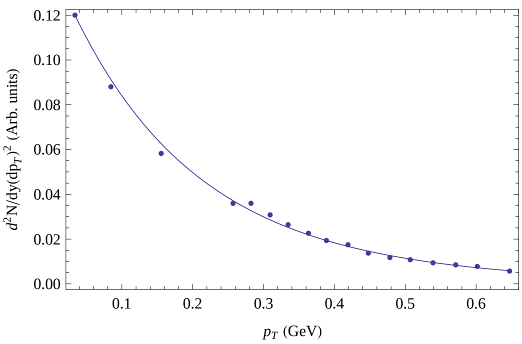

(a) p in $p - Pb$ at 450 AGeV

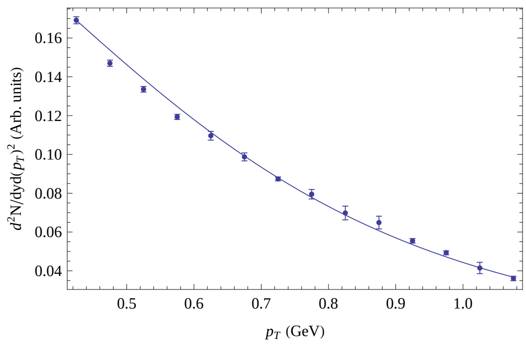

(b) p in $d - Au$ at 200 GeV

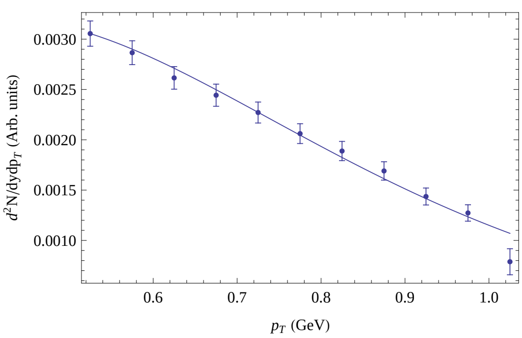

(c) p in $p - Pb$ at 5020 GeV

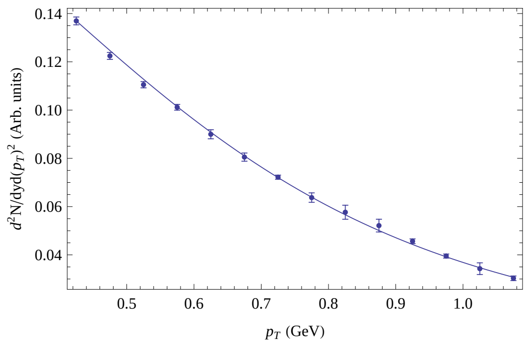

(d) $\bar{p}$ in $d - Au$ at 200 GeV

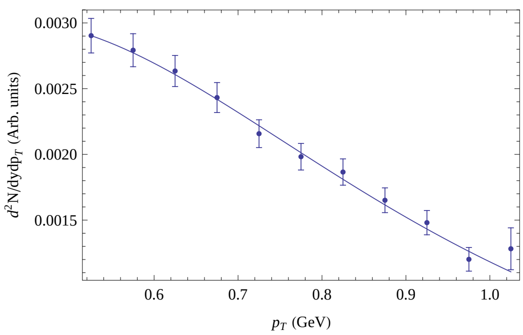

(e) $\bar{p}$ in $p - Pb$ at 5020 GeV

Figure B.3: Fits for p and $\bar{p}$ yield in $p - A$ collisions.

Appendix C

Fits of $A - A$ collisions using random walk model

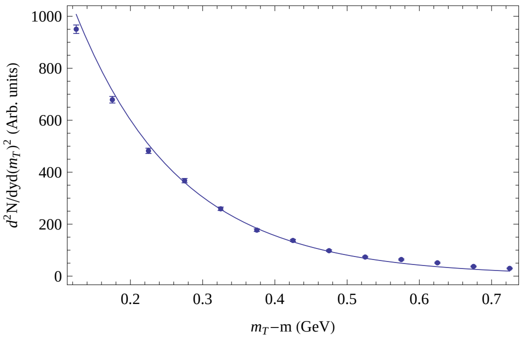

(a) π^+ in $Pb - Pb$ at 40 AGeV

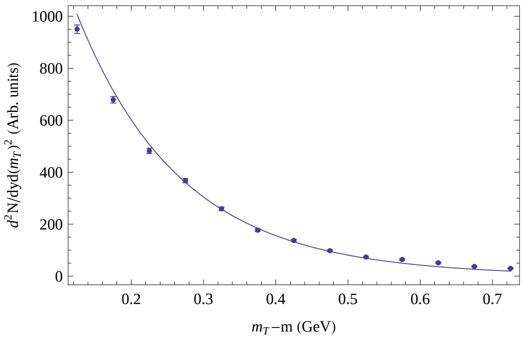

(b) π^+ in $Pb - Pb$ at 80 AGeV

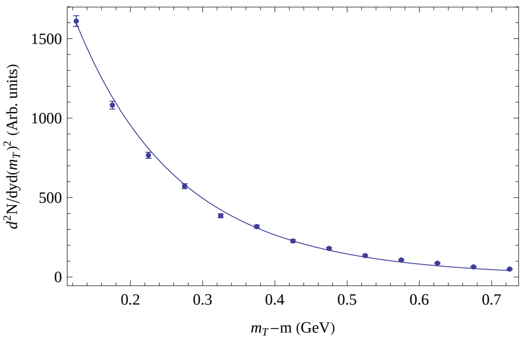

(c) π^+ in $Pb - Pb$ at 158 AGeV

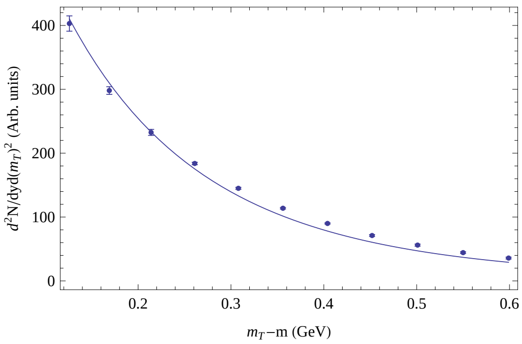

(d) π^+ in $Au - Au$ at 200 GeV

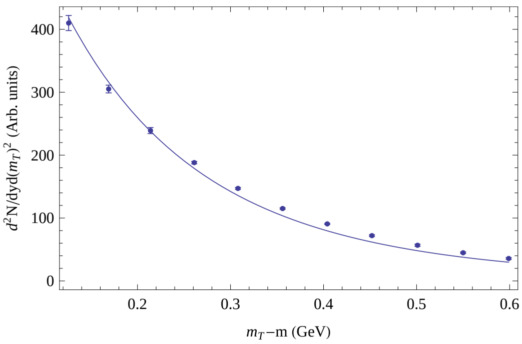

(e) π^- in $Au - Au$ at 200 GeV

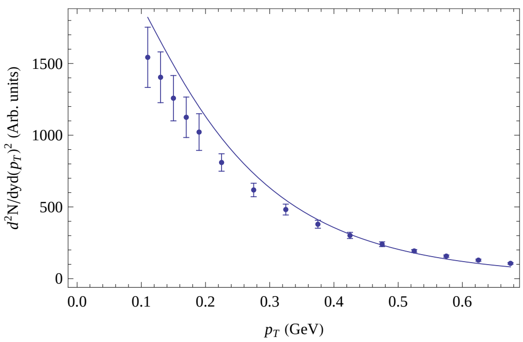

(f) π^+ in $Pb - Pb$ at 2760 GeV

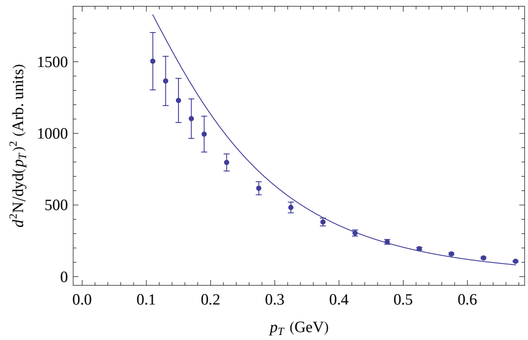

(g) π^- in $Pb - Pb$ at 2760 GeV

Figure C.1: Fits for π^+ and π^- yield in $A - A$ collisions.

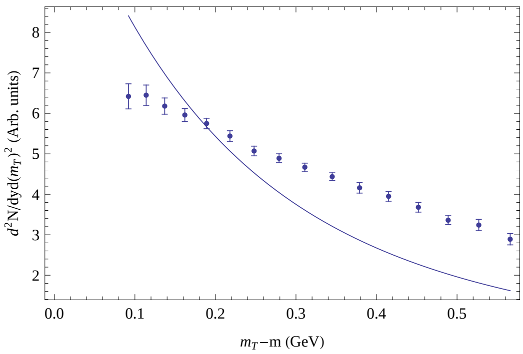

(a) p in $Au - Au$ at 200 GeV

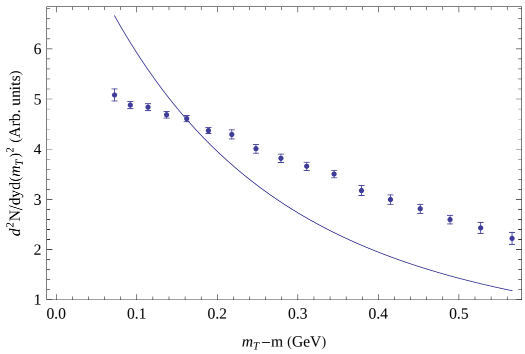

(b) $\bar{p}$ in $Au - Au$ at 200 GeV

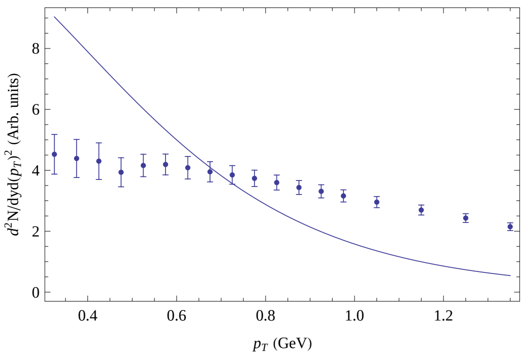

(c) p in $Pb - Pb$ at 2760 GeV

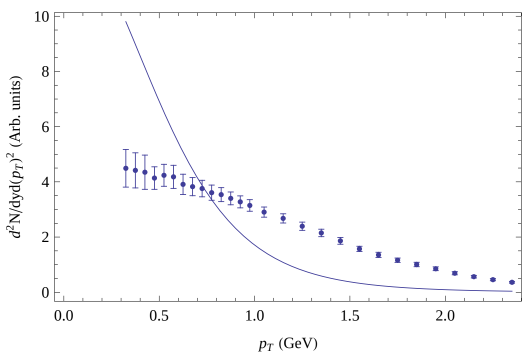

(d) $\bar{p}$ in $Pb - Pb$ at 2760 GeV

Figure C.2: Fits for p and $\bar{p}$ yield in $A - A$ collisions.

Appendix D

Fits using blast wave model

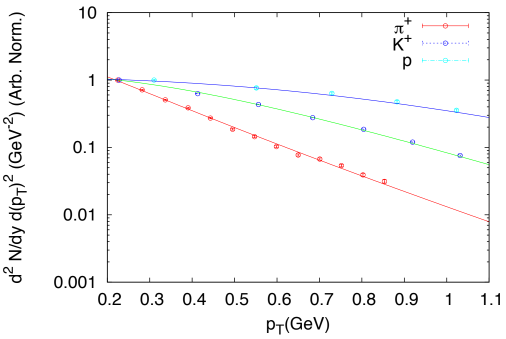

(a) $Pb - Pb$ at 40 AGeV

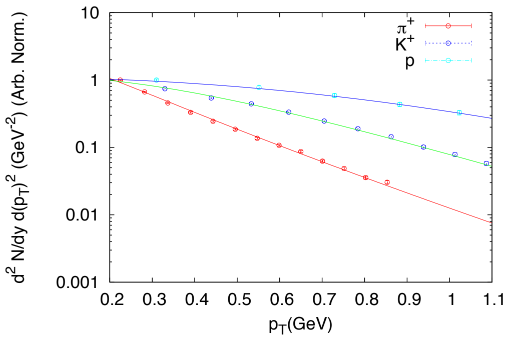

(b) $Pb - Pb$ at 80 AGeV

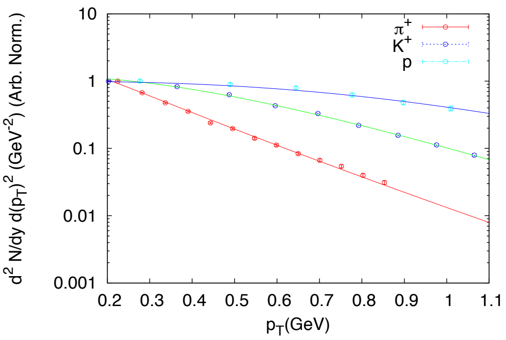

(c) $Pb - Pb$ at 158 AGeV

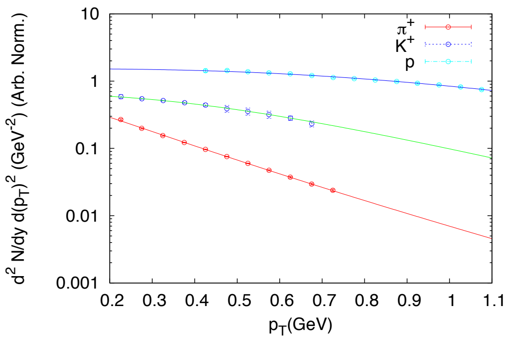

(d) $Au - Au$ at 200 GeV

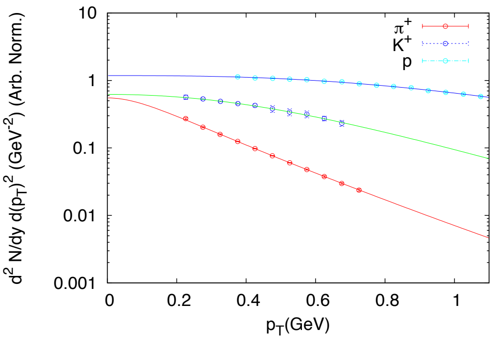

(e) $Au - Au$ at 200 GeV

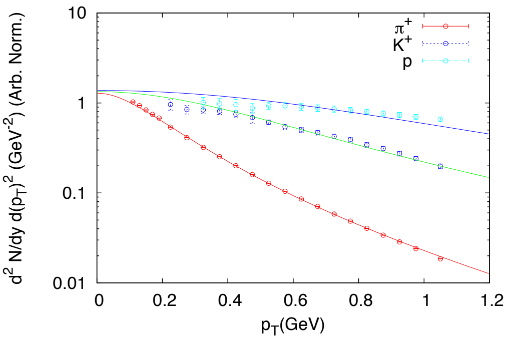

(f) $Pb - Pb$ at 2760 GeV

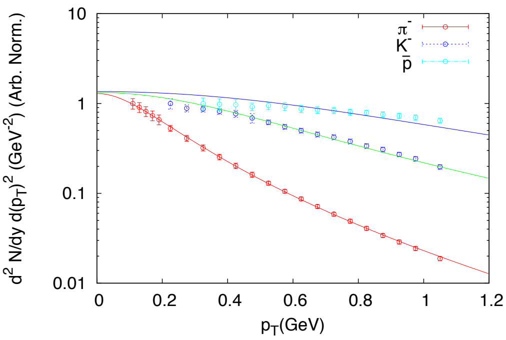

(g) $Pb - Pb$ at 2760 GeV

Figure D.1: Fits of particle yield in $A - A$ collisions using blast wave model.

Appendix E

Degrees of freedom of hadrons

Table E.1: Degrees of Freedom of Mesons[19]

Name	Mass(MeV)	Spin	Isospin	Degrees of Freedom
$\pi^{\pm}$	139.56995	0	1	3
$K^{\pm}$	493.677	0	$\frac{1}{2}$	4
η	547.3	0	0	1
ρ	770	1	1	9
ω	782	1	0	3
f_0	800	0	0	1
k^*	891.66	1	$\frac{1}{2}$	6
η'	958	0	0	1
f_0	980	0	0	1
a_0	983.4	0	1	3
Φ	1019.413	1	0	3
h_1	1170	1	0	3
b_1	1229.5	1	1	9
a_1	1230	1	1	9
f_2	1270	2	0	5
K_1	1270	1	$\frac{1}{2}$	6
η	1295	0	0	1
f_1	1281.9	1	0	3
ϕ	1300	0	1	3
a_2	1320	2	1	15
f_0	1350	0	0	1
k_1	1400	1	$\frac{1}{2}$	6
k^*	1410	1	$\frac{1}{2}$	6
ω	1420	1	0	3
f_1	1426	1	0	3
k_0^*	1429	0	$\frac{1}{2}$	2
k_2^*	1430	2	$\frac{1}{2}$	10
η	1440	0	0	1
a_0	1450	0	1	3
ρ	1450	1	1	9

f_0	1500	0	0	1
f_2'	1525	2	0	5
ω	1600	1	0	3
ω_3	1670	3	0	7
π_2	1670	2	1	15
Φ	1680	1	0	3
K^*	1680	1	$\frac{1}{2}$	6
ρ_3	1690	3	1	21
f_j	1712	0	0	1
ρ	1770	1	1	9
K_2	1770	2	$\frac{1}{2}$	10
K_3^*	1780	3	$\frac{1}{2}$	14
Pi	1800	0	1	3
K_2	1820	2	$\frac{1}{2}$	10
Φ_3	1850	3	0	7
f_3	2010	2	0	5
a_4	2040	4	1	27
K_4^*	2045	4	$\frac{1}{2}$	18
f_4	2050	4	0	9
f_2	2300	2	0	5
f_2	2340	2	0	5

Table E.2: Degrees of Freedom of Baryons[19]

Name	Mass(MeV)	Spin	Isospin	Degrees of Freedom
p	938.27231	$\frac{1}{2}$	$\frac{1}{2}$	4
Λ	1115.683	$\frac{1}{2}$	0	2
Σ	1189.37	$\frac{1}{2}$	1	5
Δ	1232	$\frac{3}{2}$	$\frac{3}{2}$	16
Ξ^0	1314.9	$\frac{1}{2}$	$\frac{1}{2}$	4
Σ	1385	$\frac{3}{2}$	1	12
Λ	1407	$\frac{1}{2}$	0	2
N	1440	$\frac{1}{2}$	$\frac{1}{2}$	4
Λ	1519.5	$\frac{3}{2}$	0	4
N	1520	$\frac{3}{2}$	$\frac{1}{2}$	8
Ξ	1531.80	$\frac{3}{2}$	$\frac{1}{2}$	8
N	1535	$\frac{1}{2}$	$\frac{1}{2}$	4
Λ	1600	$\frac{1}{2}$	0	2
Δ	1600	$\frac{3}{2}$	$\frac{3}{2}$	16
Δ	1620	$\frac{1}{2}$	$\frac{3}{2}$	8
N	1650	$\frac{1}{2}$	$\frac{1}{2}$	4

Σ	1660	$\frac{1}{2}$	1	6
Λ	1670	$\frac{1}{2}$	0	2
Σ	1670	$\frac{3}{2}$	1	12
Ω	1672.45	$\frac{3}{2}$	0	5
N	1675	$\frac{5}{2}$	$\frac{1}{2}$	12
N	1680	$\frac{5}{2}$	$\frac{1}{2}$	12
Λ	1690	$\frac{3}{2}$	0	4
N	1700	$\frac{3}{2}$	$\frac{1}{2}$	8
Δ	1700	$\frac{3}{2}$	$\frac{3}{2}$	16
N	1710	$\frac{1}{2}$	$\frac{1}{2}$	4
N	1720	$\frac{3}{2}$	$\frac{1}{2}$	8
Σ	1750	$\frac{1}{2}$	1	6
Σ	1775	$\frac{5}{2}$	1	18
Λ	1800	$\frac{1}{2}$	0	2
Λ	1810	$\frac{1}{2}$	0	2
Λ	1820	$\frac{5}{2}$	0	6
Ξ	1820	$\frac{3}{2}$	$\frac{1}{2}$	8
Λ	1830	$\frac{5}{2}$	0	6
Λ	1890	$\frac{3}{2}$	0	4
Δ	1905	$\frac{5}{2}$	$\frac{3}{2}$	24
Δ	1910	$\frac{1}{2}$	$\frac{3}{2}$	8
Σ	1915	$\frac{5}{2}$	1	18
Δ	1920	$\frac{3}{2}$	$\frac{3}{2}$	16
Δ	1930	$\frac{5}{2}$	$\frac{3}{2}$	24
Σ	1940	$\frac{3}{2}$	1	12
Δ	1950	$\frac{7}{2}$	$\frac{3}{2}$	32
Σ	2030	$\frac{7}{2}$	1	24
Λ	2100	$\frac{7}{2}$	0	8
Λ	2110	$\frac{5}{2}$	0	6
N	2190	$\frac{9}{2}$	$\frac{1}{2}$	16
N	2220	$\frac{9}{2}$	$\frac{1}{2}$	20
N	2250	$\frac{9}{2}$	$\frac{1}{2}$	20
Λ	2350	$\frac{9}{2}$	0	10
Δ	2420	$\frac{11}{2}$	$\frac{3}{2}$	48
N	2600	$\frac{11}{2}$	$\frac{1}{2}$	24